

ON THE FORMATION AND ISOMER SPECIFIC DETECTION OF PROPENAL (C₂H₃CHO) AND CYCLOPROPANONE (c-C₃H₄O) IN INTERSTELLAR MODEL ICES—A COMBINED FTIR AND REFLECTRON TIME-OF-FLIGHT MASS SPECTROSCOPIC STUDY

MATTHEW J. ABPLANALP^{1,2}, ALECA BORSUK¹, BRANT M. JONES^{1,2}, AND RALF I. KAISER^{1,2}

¹ W. M. Keck Research Laboratory in Astrochemistry, University of Hawaii at Manoa, Honolulu, Hawaii, HI, 96822, USA; ralfk@hawaii.edu

² Department of Chemistry, University of Hawaii at Manoa, Honolulu, Hawaii, HI, 96822, USA

Received 2015 May 9; accepted 2015 October 12; published 2015 November 16

ABSTRACT

The formation routes of two structural isomers—propenal (C₂H₃CHO) and cyclopropanone (c-C₃H₄O)—were investigated experimentally by exposing ices of astrophysical interest to energetic electrons at 5.5 K thus mimicking the interaction of ionizing radiation with interstellar ices in cold molecular clouds. The radiation-induced processing of these ices was monitored *online* and in situ via Fourier Transform Infrared spectroscopy and via temperature programmed desorption exploiting highly sensitive reflectron time-of-flight mass spectrometry coupled with single photon ionization in the post irradiation phase. To selectively probe which isomer(s) is/are formed, the photoionization experiments were conducted with 10.49 and 9.60 eV photons. Our studies provided compelling evidence on the formation of both isomers—propenal (C₂H₃CHO) and cyclopropanone (c-C₃H₄O)—in ethylene (C₂H₄)—carbon monoxide (CO) ices forming propenal and cyclopropanone at a ratio of (4.5 ± 0.9):1. Based on the extracted reaction pathways, the cyclopropanone molecule can be classified as a tracer of a low temperature non-equilibrium chemistry within interstellar ices involving most likely excited triplet states, whereas propenal can be formed at ultralow temperatures, but also during the annealing phase via non-equilibrium as well as thermal chemistry (radical recombination). Since propenal has been detected in the interstellar medium and our laboratory experiments demonstrate that both isomers originated from identical precursor molecules our study predicts that the hitherto elusive second isomer—cyclopropanone—should also be observable toward those astronomical sources such as Sgr B2(N) in which propenal has been detected.

Key words: astrochemistry – cosmic rays – infrared: general – ISM: molecules – methods: laboratory: solid state – radiation mechanisms: non-thermal

1. INTRODUCTION

Since the detection of the simplest sugar glycolaldehyde (HCOCH₂OH) in the interstellar medium (ISM) toward Sgr B2 (N) (Hollis et al. 2000), complex organic molecules (COMs) such as aldehydes (RCHO) and ketones (R'COR) have gained substantial interest from the astrochemistry and astrobiology communities as aldehydes and ketones are structurally closely related to aldose and ketose sugars (Hollis et al. 2000; Kaiser et al. 2014; Jaber et al. 2014; de Marcellus et al. 2015). The understanding of the formation routes of COMs provides substantial information on the chemical evolution of cold molecular clouds, hot molecular cores, and star-forming regions (Minh & van Dishoeck 2000) since structural isomers in particular—molecules with the same chemical formula but different connectivities of atoms—act as a “chemical clock” to define the interstellar environment’s chemical and physical conditions (Kaiser 2002). Figure 1 shows the structures of the C₃H₄O isomers propenal (C₂H₃CHO) and cyclopropanone (c-C₃H₄O) which are specifically interesting isomers because only propenal has so far been detected in the ISM, while other similar pairs of isomers have both been detected. Dickens et al. (2001) first observed interstellar propenal in the hot core region G327.3–0.6 and Sgr B2(N); since then, propenal has been detected in multiple line surveys (Ureña et al. 2003; Hollis et al. 2004; Requena-Torres et al. 2008; Sigurbjornsson & Signorell 2008; Wang et al. 2010) with fractional abundances of 6.3 × 10^{−9}, 0.3 × 10^{−9}, 2.3 × 10^{−9}, and 0.9 × 10^{−9} for NGC 7129-FIRS2, G−0.02, G−0.11, and G+0.693, respectively. However, the cyclic isomer cyclopropanone still remains

undetected. This case becomes even more interesting as a structurally related isomer pair propynal (HCCCHO) and cyclopropenone (c-C₃H₂O) (Figure 1) have been detected in the ISM toward TMC-1 and Sgr B2(N-LMH) with fractional abundances of 1.5 × 10^{−10}, and 6 × 10^{−11}, respectively, (Irvine et al. 1988; Hollis et al. 2006), and also in the laboratory in irradiated acetylene (C₂H₂)—carbon monoxide (CO) interstellar model ices (Zhou et al. 2008).

Although propenal has been detected in the ISM more than a decade ago, its formation route is still not understood (Herbst 2014). When Dickens et al. (2001) first identified interstellar propenal, the authors proposed that this molecule could be the result of ill-defined gas-grain chemistry; but no models were provided. Hollis et al. (2004) speculated then that with the firm detection of propanal and propynal in Sgr B2(N), propenal can be formed via hydrogen addition reactions (Hudson & Moore 1999; Moore & Hudson 2005). Requena-Torres et al. (2008) stated that it is unlikely that COMs are synthesized via gas phase reactions; specifically these authors speculated that propenal forms from the hydrogenation of propynal on grains. Rawlings et al. (2013) recently suggested that an explosive desorption of ice layers of interstellar grains results in the gas-phase production of propenal from the formyl radical (HCO) and vinyl radical (C₂H₃) in a three body collision with water (H₂O), however, the authors neglected that under these conditions, termolecular reactions are highly unlikely and only bimolecular reactions should take place. Finally, it is important to highlight that the *cis*- and *trans*-forms of propenal were apparently generated via broad band

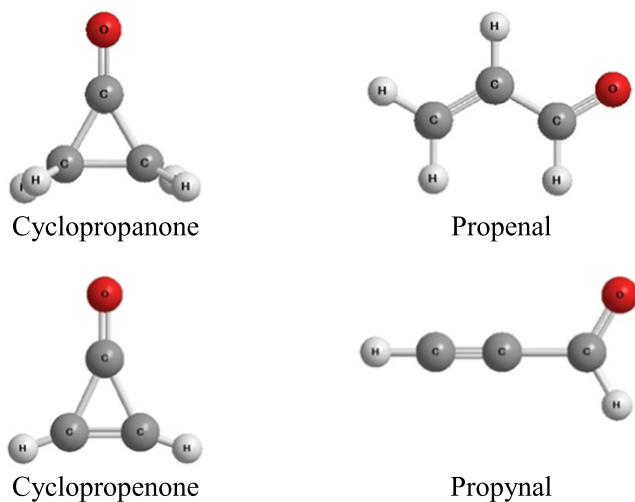


Figure 1. Structures of two pairs of isomers: C_3H_4O isomers cyclopropanone and propenal (the isomers of focus for the following experiments), and C_3H_2O isomers propynal and cyclopropenone. Of the molecules above cyclopropanone remains to be the only undetected molecule in the ISM.

ultraviolet (UV) irradiation of water-methanol-ammonia (H_2O - $^{13}CH_3OH$ - NH_3 ; 12:3.5:1) with a hydrogen microwave-discharge lamp and tentatively detected in the organic residues exploring gas chromatography coupled to a time-of-flight mass spectrometer; cyclopropanone was not identified in the residue (de Marcellus et al. 2015) most likely due to the instability of this molecule, which easily decomposes at elevated temperatures. Nevertheless, formation routes of both structural isomers via interaction of ionizing radiation such as UV photons and/or galactic cosmic rays with interstellar analog ices has not been explored to date although the exposure of ionizing radiation to low temperature ices has been well established to induce non-equilibrium chemistry inside the bulk of the interstellar ices (Kaiser et al. 1997; Kaiser & Roessler 1998; Bennett et al. 2005a; Geppert et al. 2006; Mason et al. 2006; Bisschop et al. 2007; Garozzo et al. 2010) leading to COMs. These are for instance the C_2H_4O and $C_2H_4O_2$ isomers acetaldehyde ($HCOCH_3$), vinyl alcohol (CH_2CHOH), and ethylene oxide ($c-C_2H_4O$) (Gilmore et al. 1976; Dickens et al. 1997; Moore & Hudson 1998; Turner & Apponi 2001; Bennett et al. 2005a, 2005b; Kaiser et al. 2014; Maity et al. 2015) as well as acetic acid (CH_3COOH), methyl formate ($HCOOCH_3$), and glycolaldehyde ($HCOCH_2OH$) (Brown et al. 1975; Mehringer et al. 1997; Hollis et al. 2000; Bennett et al. 2007; Bennett & Kaiser 2007a, 2007b; Kim & Kaiser 2010; Maity et al. 2014b, 2015), respectively. Once these COMs are formed inside the ices at 10 K via non-equilibrium chemistry, they can then sublime into the gas phase as the temperature increases when the cold molecular cloud transitions into star-forming regions. Therefore, as the synthetic routes to the formation of propenal (C_2H_3CHO) and cyclopropanone ($c-C_3H_4O$) are still unknown, a novel experimental approach to elucidate the formation of these C_3H_4O isomers is desirable.

2. EXPERIMENTAL STRATEGY

The present study experimentally investigated the formation of propenal (C_2H_3CHO) and cyclopropanone ($c-C_3H_4O$) within non-polar interstellar ice analogs consisting of carbon monoxide (CO) and ethylene (C_2H_4). Carbon monoxide (CO) is a well-known component of interstellar ices reaching levels of

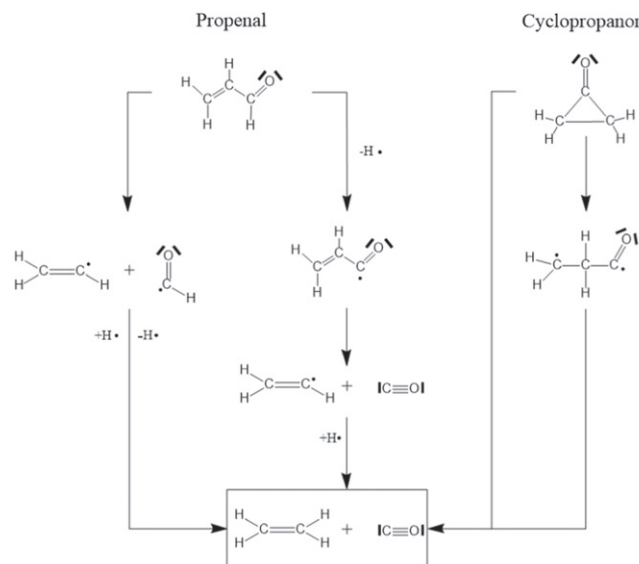


Figure 2. Retrosynthesis of the two C_3H_4O isomers of interest, which shows that either isomer may be formed from the processing of carbon monoxide-ethylene ice.

25% (Gibb et al. 2004); ethylene (C_2H_4) has been shown in laboratory experiments to be formed easily in irradiated methane (CH_4) ices (Bennett et al. 2006), which is present in interstellar ices at levels up to 4% (Gibb et al. 2004). The starting mixture of carbon monoxide (CO)-ethylene (C_2H_4) was chosen by performing a retrosynthesis (Figure 2; Bennett et al. 2005a) of the isomers of interest. This retrosynthesis predicts that both isomers can be synthesized from the closed shell reactants carbon monoxide (CO) and ethylene (C_2H_4) via stepwise and/or concerted reaction mechanisms.

Which analytical technique can be exploited to probe the formation of these structural isomers online and in situ? First, Fourier Transform Infrared spectroscopy (FTIR) has been extensively used to monitor astrophysical ice analogs in the laboratory; however, the ability of infrared spectroscopy to provide useful information for the detection of COMs formed within the ices is quite limited (Khare et al. 1989; Moore et al. 1996; Caro & Schutte 2003; Jones & Kaiser 2013; Kaiser et al. 2014, 2015; Maity et al. 2014a, 2014b, 2015). Here, infrared spectroscopy allows the functional groups of COMs to be identified; however, this information does not always identify individual molecules since the functional groups of, for instance, carbonyls like aldehydes and ketones depict similar fundamental modes from 1850 to 1600 cm^{-1} . Therefore, the exclusive assignment of a single molecule to infrared bands in an unknown mixture of COMs is not acceptable. To be more specific, the carbonyl stretching modes of propenal (C_2H_3CHO) and cyclopropanone ($c-C_3H_4O$) absorb at 1684 cm^{-1} and 1816 cm^{-1} , respectively (Fujii et al. 1995; Breda et al. 2012). These peak positions fall within a range of saturated and unsaturated aldehydes and ketones from 1850 to 1600 cm^{-1} (Socrates 2004) thus making it impossible to identify propenal (C_2H_3CHO) and cyclopropanone ($c-C_3H_4O$) within a complex mixtures of aldehydes and ketones. Due to these restrictions, FTIR aids in identifying new functional groups of COMs formed within the astrophysical ice analogs, but FTIR cannot always identify the isomers of interest.

Second, mass spectrometry exploiting a quadrupole mass spectrometer (QMS) coupled with electron impact ionization of

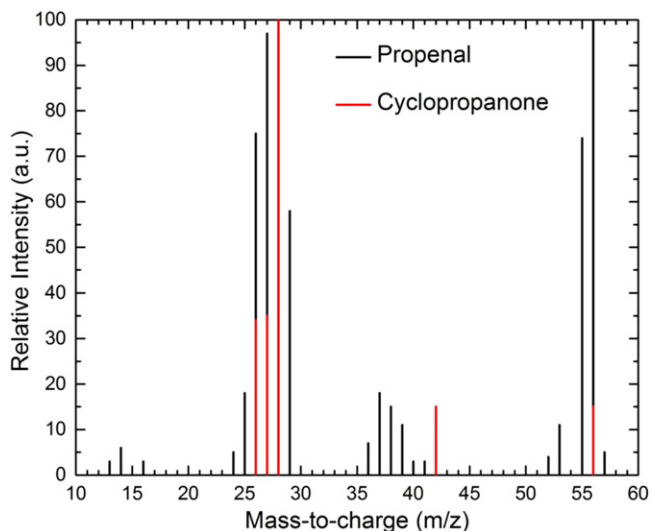


Figure 3. Comparison of the electron impact ionization mass spectra from the isomers propenal and cyclopropanone, as reported by Stein (2010) and Rothgery et al. (1975), respectively.

the subliming molecules during temperature programmed desorption (TPD) has been used to identify newly formed molecules in the processed ices after their sublimation into the gas phase. However, the QMS using an electron impact ionizer operating at 100 eV electron energy does not only ionize molecules, but also significantly fragments the newly formed species. In the worst case, this can lead to the absence of the molecular parent ion. Likewise, the fragment ions of structural isomers often overlap making it difficult to decipher and to even discriminate between structural isomers such as propenal (C_2H_3CHO) and cyclopropanone ($c-C_3H_4O$) (Figure 3).

Therefore, traditional methods utilized to identify COMs in irradiated interstellar analog ices fall short to detect specific isomers. Consequently, an alternative method to understand the complexity of the chemistry taking place in these ices is needed. The present study exploits for the first time tunable photoionization coupled with reflectron-time-of-flight mass spectrometry (PI-ReTOF-MS), which has been shown to be a very useful technique using a single photoionization energy of 10.49 eV (Jones & Kaiser 2013; Kaiser et al. 2014, 2015; Maity et al. 2014a, 2014b, 2015). First, by softly photoionizing the subliming molecules by a single vacuum ultraviolet (VUV) photon, fragmentation of the molecular ion can be primarily avoided. Second, by tuning the photon energy and following the change in the TPD profile of the molecular ion peak of the molecule of interest, it is feasible to selectively photoionize only one isomer and to discriminate—if overlapping structures are present in the TPD process—the nature of the structural isomer(s) formed. In the present case, propenal (C_2H_3CHO) and cyclopropanone ($c-C_3H_4O$) have distinct ionization energies of 10.10 eV and 9.10 eV, respectively (Watanabe 1957; Rothgery et al. 1975); this is expected to result in distinct peaks at the molecular parent at $m/z = 56$. Unfortunately, irradiation of ethylene bearing ices also forms butene (C_4H_8) (Zhou et al. 2014) ($m/z = 56$); this would interfere with the signal from the newly formed propenal (C_2H_3CHO) and cyclopropanone ($c-C_3H_4O$), if traditional electron impact ionization is used. However, since the ionization energy of 1-butene (9.55 eV) (Adam & Zimmermann 2007) falls between the ionization energies of propenal (C_2H_3CHO) and

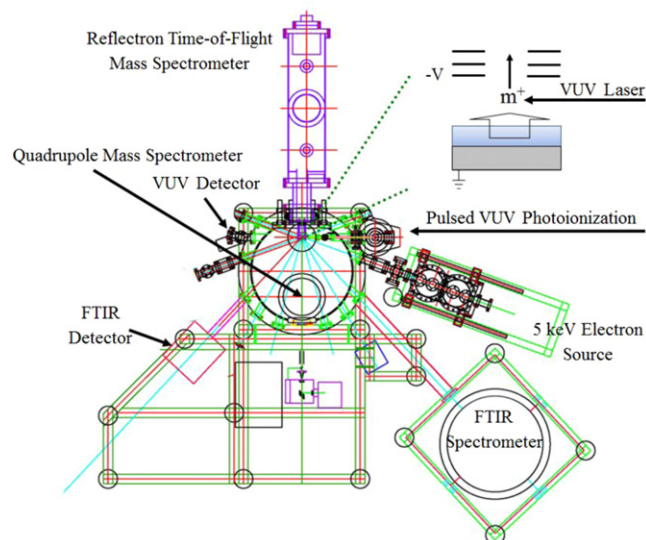


Figure 4. Schematic top view of the main chamber including the analytical instruments, radiation source, and the cryogenic target (point of converging lines). The alignment of the cryogenic target, radiation source, and infrared spectrometer allows simultaneous online and in situ measurements of the modification of the targets upon the irradiation exposure. After the irradiation, the cold head can be rotated 180° to face the ReTOF mass spectrometer; the target can then be heated allowing the newly formed products to sublimate where upon they are photoionized and mass analyzed. The inset (top right) shows the geometry of the ReTOF ion source lenses with respect to the target and ionization laser.

cyclopropanone ($c-C_3H_4O$), the ionization energy of the photons can be tuned to discriminate between propenal (C_2H_3CHO), cyclopropanone ($c-C_3H_4O$), and butene (C_4H_8). In summary, tunable photoionization allows for the molecular ion to remain intact as the “soft” ionization method ideally does not result in major fragmentation; further, this approach has the capability of specific molecules to be ionized and hence to be detected based on their distinct ionization energy by tuning the photoionization energy. Finally, selective isotopically labeled ices ($CO-C_2H_4$, $C^{18}O-C_2H_4$, $CO-C_2D_4$, $C^{18}O-C_2D_4$) were also investigated to confirm assignments of the newly formed molecules due to their shifts in mass-to-charge ratios upon labeling.

3. EXPERIMENTAL

The experiments were performed in a contamination free ultrahigh vacuum (UHV) chamber at the W. M. Keck Research Laboratory in Astrochemistry (Figure 4) operating at base pressures of a few 10^{-11} Torr using magnetically suspended turbo molecular pumps operating parallel and in series backed by oil free scroll pumps (Jones & Kaiser 2013; Kaiser et al. 2014). A polished silver mirror acts as the substrate; the latter is interfaced to a cryogenically cooled target (“cold finger”) machined from oxygen free high conductivity copper (OFHC) with indium foil to ensure uniform thermal conductivity when cooled to 5.5 ± 0.1 K exploiting a UHV compatible closed-cycle helium compressor (Sumitomo Heavy Industries, RDK-415E). The substrate is freely rotatable within the horizontal plane via a differential pumped rotational feedthrough (Thermoionics Vacuum Products, RNN-600/FA/MCO) and also translatable in the vertical axis through a UHV compatible bellow (McAllister, BLT106).

Gas mixtures of carbon monoxide (CO, Aldrich, 99.99%) and ethylene (C₂H₄, Linde, 99.999%) with partial pressures of 60 and 50 Torr were premixed in a gas mixing chamber and introduced into the main chamber at a background pressure of 5×10^{-8} Torr for 10 minutes through a glass capillary array held 30 mm in front of the silver mirror (Maity et al. 2014a). The ice thickness was determined in situ via laser interferometry (Heavens 1965; Groner et al. 1973) to be 550 ± 20 nm with a helium-neon (HeNe) laser (CVI Melles-Griot; 25-LHP-230) operating at 632.8 nm and using an index of refraction of the mixed ice of 1.32 ± 0.02 derived from numerical fitting of the intensity ratios (Goodman 1978). Exploiting a modified Lambert–Beer relationship (Moore et al. 2001; Bennett et al. 2004; Wada et al. 2006) with absorption coefficients of 1.1×10^{-17} cm molecule⁻¹ and 1.0×10^{-18} cm molecule⁻¹ for the 2090 cm⁻¹ (ν_1 , ¹³CO) (Garozzo et al. 2010) and 2977 cm⁻¹ (ν_{11} , C₂H₄) (Cowieson et al. 1981; Hudson et al. 2014) bands, a total ice thickness of 530 ± 100 nm was determined, which is in agreement with the data from the laser interferometry. The ratio (CO:C₂H₄) of the ice composition was determined to be $1.0 \pm 0.2:1.7 \pm 0.6$ using the above absorption coefficients to monitor the contribution of each chemical to the ice composition. Isotopic mixtures of C¹⁸O–C₂H₄, CO–C₂D₄, and C¹⁸O–C₂D₄ (C¹⁸O, Aldrich, 99.9%-¹⁸O; C₂D₄, CDN Isotopes, 99.8%-D) were investigated to confirm infrared assignments via isotopic shifts and to investigate the mass spectroscopic data via their change in the corresponding mass-to-charge ratios upon isotopic substitution.

Once the ice of a well-defined thickness was prepared on the substrate, each ice mixture was exposed to 5 keV electrons for 60 minutes at 30 nA over an area of 1.0 ± 0.1 cm² at an angle of incidence of 70° relative to the surface normal of the substrate. The averaged penetration depth of the energetic electrons was calculated via Monte Carlo simulations (CASINO) (Drouin et al. 2007) to be 320 ± 20 nm. This penetration depth is less than the thickness of the deposited ices of 550 ± 20 nm to insure that the energetic electrons only interact with the ices and not with the silver substrate. The dose deposited into the ice sample was determined on average to be 3.6 ± 0.7 eV per CO molecule and 4.9 ± 0.9 eV per C₂H₄ molecule. These dosage values are calculated utilizing the densities of 1.03 g cm⁻³ (Jiang et al. 1975) and 0.75 g cm⁻³ (van Nes 1978) for carbon monoxide and ethylene, respectively.

The chemical evolution of the irradiated ices was monitored online and in situ during the irradiation via a FTIR spectrometer (Nicolet 6700) from 6000 to 500 cm⁻¹ with a resolution of 4 cm⁻¹ in intervals of 2 minutes; this results in 30 spectra during the radiation exposure. The sample is then kept isothermal at 5.5 K for 1 hr after irradiation before TPD studies were conducted to sublime the ice and any products by warming up the irradiated samples to 300 K at a rate of 0.5 K minutes⁻¹. During the TPD process, the samples can be also monitored via FTIR spectroscopy. The subliming molecules were probed with a reflectron time-of-flight mass spectrometer (Jordan TOF Products, Inc.) coupled with soft photoionization upon photoionization of the neutral molecules. In detail, the products were analyzed via single photon ionization using pulsed (30 Hz) coherent VUV light at 118.2 nm (10.49 eV) (Kaiser et al. 2014; Maity et al. 2014a, 2014b) and 129.15 nm (9.60 eV). Considering the ionization energies of propenal (10.10 eV) (Watanabe 1957) and of cyclopropanone (9.10 eV) (Rothgery et al. 1975),

photoionization at 10.49 eV should photoionize *both* isomers, whereas photoionization at 9.60 eV *selectively* photoionizes cyclopropanone.

The photoionized molecules were then extracted and directed toward the focusing regions by holding the substrate, acting as the repeller plate, at ground and applying a voltage to the extraction plate (−190 V) to create a constant negative field between the repeller and extraction plates (−210 V). The photoionized molecules were then detected via a multichannel plate in the dual chevron configuration based upon the time of arrival. These signals were then amplified with a fast preamplifier (Ortec 9305) and shaped with a 100 MHz discriminator. The time-of-flight spectra are recorded with a personal-computer-based-multichannel scalar (FAST ComTec, P7888-1 E) with a bin width of 4 ns which is triggered at 30 Hz (Quantum Composers, 9518) and 3600 sweeps per mass spectrum correlated with a 1 K change during the TPD study.

4. RESULTS

4.1. Infrared Spectroscopy

Figure 5(a) displays the infrared spectra of the binary ice consisting of carbon monoxide (CO) and ethylene (C₂H₄) before and after irradiation with absorption assignments at 5.5 K given in Table 1; these are confirmed with the corresponding isotopic shifts compiled in Table 2. Briefly, Figure 5(b) zooms into the 1800 to 1600 cm⁻¹ region of Figure 5(a), this region covers the carbonyl stretching (Socrates 2004). The same region is also shown in Figure 5(c) for ¹⁸O–carbon monoxide (C¹⁸O) and D₄–ethylene (C₂D₄), which clearly shows a shift in the peak positions due to the isotopic labeling. Also, Figure 5(d) portrays this region for a pure D₄–ethylene ice (C₂D₄), which exhibits no detectable peaks and confirms the absorptions detected in the above mixtures to be directly dependent on the binary carbon monoxide–ethylene ice mixtures.

As these absorptions are broad and not well defined it was necessary to perform a deconvolution to discriminate how many peaks were truly represented by these absorptions. GRAMS-AI software was used to deconvolute the spectra by iterative fitting of the spectra with Gaussian shaped peaks using the fewest number of fitting peaks to compute a fit that resulted in a residual within the signal-to-noise ratio of the original spectra. Figures 5(e) and (f) exhibit the deconvoluted spectra for the irradiated CO–C₂H₄ and C¹⁸O–C₂D₄ ice mixtures, respectively. Finally, Figure 5(g) presents an overlay of the irradiated CO–C₂H₄ ice, the deconvoluted peak at 1696 cm⁻¹, and the infrared spectrum of 1% propenal (as a calibration compound) in the CO–C₂H₄ ice. Here, the overlap of the strong propenal fundamental with the position of the 1696 cm⁻¹ peak of the irradiated sample is very strong. Fujii et al. (1995) assigned an absorption at 1684 cm⁻¹ to the carbonyl stretch (C=O) of propenal. Further, the formyl radical—the building block of propenal—can be attributed in the irradiated ices via its carbonyl stretching mode at 1845 cm⁻¹ (Bennett & Kaiser 2007a).

With respect to cyclopropanone, Breda et al. (2012) assigned an absorption at 1816 cm⁻¹ to the carbonyl stretch (C=O) of cyclopropanone in a xenon matrix at 30 K; however, this absorption can also overlap with the carbonyl stretch (C=O) of the hydroxycarbonyl (HOCO) radical, which we detect based on isotopic shifts at 1823 cm⁻¹ in the irradiated samples. In

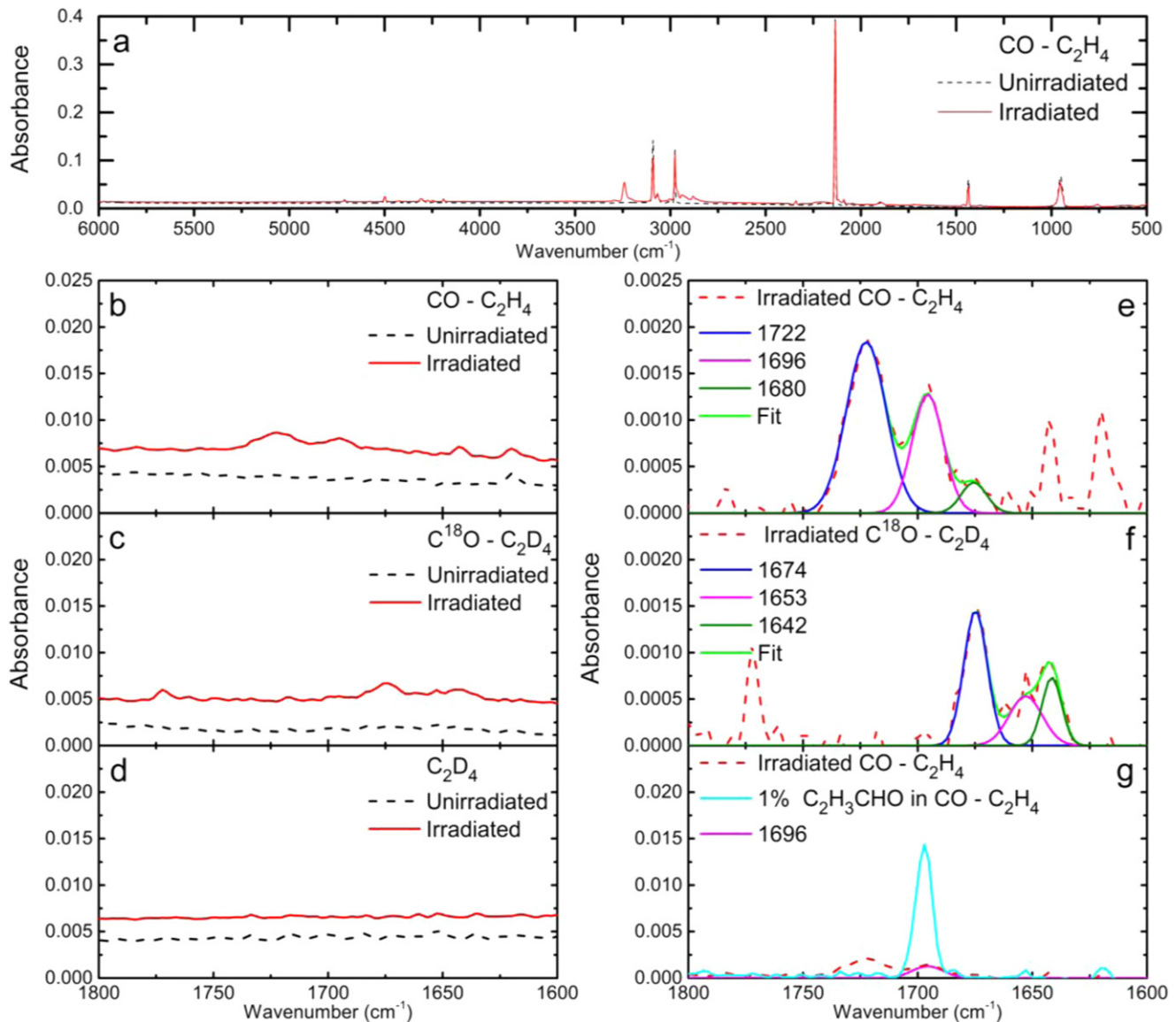


Figure 5. Infrared spectra of carbon monoxide-ethylene ices. (a) Infrared spectrum of CO-C₂H₄ before (black dashed line) and after (red solid line) the irradiation; peak assignments in Table 1(a). (b) The 1800–1600 cm⁻¹ region of CO-C₂H₄ zoomed in to show carbonyl features before (black dashed line) and after (red solid line) the irradiation. (c) The 1800–1600 cm⁻¹ region of C¹⁸O-C₂D₄ before (black dashed line) and after (red solid line) the irradiation. (d) The 1800–1600 cm⁻¹ region of C₂D₄ before (black dashed line) and after (red solid line) the irradiation. (e) Deconvolution of the 1800–1600 cm⁻¹ region of CO-C₂H₄ to show specific carbonyl features (peak centers shown in graph) after (red dashed line) the irradiation. (f) Deconvolution of the 1800–1600 cm⁻¹ region of C¹⁸O-C₂D₄ to show specific carbonyl features (peak centers shown in graph) after (red dashed line) the irradiation. (g) An overlay of the 1800–1600 cm⁻¹ region of: 1% propenal (C₂H₃CHO) in unirradiated CO-C₂H₄ ice (cyan trace), irradiated CO-C₂H₄ (red), and a deconvoluted peak of the irradiated CO-C₂H₄ centered at 1696 cm⁻¹ (pink).

summary, although the 1696 and 1822 cm⁻¹ absorptions together with their shifted frequencies in irradiated isotopically labeled ices might be assigned to propenal and cyclopropanone, respectively, these absorptions are not unique, and an alternative analytical tool is necessary, i.e., PI-ReTOF-MS as discussed above.

Since the ice is continuously monitored during both the irradiation and the warm-up phase of the ice via infrared spectroscopy and also through photoionization of the subliming gas molecules, the detection of subliming molecules in the gas phase via their molecular ions can be correlated with the decrease in intensity of their absorptions in the infrared spectra. The changes of the infrared spectra during TPD are shown in Figures 6(a)–(f), displaying the infrared spectra at 10, 70, 125, 180, 200, 250, and 300 K. However, Figure 6 shows that there

must be contributions from multiple COMs carrying the carbonyl functional group than just the propenal and cyclopropanone as the PI-ReTOF-MS signal corresponding to propenal and/or cyclopropanone is no longer detectable at temperatures larger than 180 K (Section 4.2). This suggests that larger molecular weight molecules contain a carbonyl function, to be identified in a forthcoming publication, are clearly formed during the irradiation of the ices.

4.2. PI-ReTOF-MS

The formation of larger molecular weight molecules is substantiated via the PI-ReTOF-MS study (Figure 7(a); CO-C₂H₄ system). Figure 7(a) is a visualization of the intensities of the ion counts at each mass-to-charge (mass spectrum) at each temperature up to 300 K obtained by photoionizing the

Table 1
Infrared Absorption Features Recorded Before and After the Irradiation of Carbon Monoxide–Ethylene Ices (CO–C₂H₄) at 5.5 K

Absorptions Before Irradiation (cm ⁻¹)	Absorptions After Irradiation (cm ⁻¹)	Assignment	Carrier	References
4746, 4710, 4578, 4500, 4426, 4396, 4310, 4275, 4192	...	$\nu_9 + 2\nu_6, \nu_9 + \nu_2, \nu_{11} + \nu_2, \nu_5 + \nu_{12}, \nu_9 + \nu_3, \nu_9 + \nu_6, \nu_{11} + \nu_3, \nu_{11} + \nu_6$ (C ₂ H ₄)	Overtone/Combinations	(1), (2)
4248	...	$2\nu_1$ (CO)	Overtone	(3), (6), (14)
...	3300	ν_3 (C ₂ H ₂)	CH stretch	(4), (7)
...	3245	ν_3 (C ₂ H ₂)	CH stretch	(4), (5), (12)
3092	...	ν_9 (C ₂ H ₄)	CH ₂ asymmetric stretch	(2), (7), (9), (10)
3069	...	$\nu_2 + \nu_{12}$ (C ₂ H ₄)	Combination	(2), (10)
2977	...	ν_{11} (C ₂ H ₄)	CH ₂ symmetric stretch	(2), (7), (8), (10)
...	2965	ν_{12} (C ₄ H ₁₀)/ ν_{10} (C ₂ H ₆)/ ν_{16} (C ₄ H ₈)	CH ₃ stretch	(4), (5), (11), (13), (15), (18)
...	2940	$\nu_8 + \nu_{11}$ (C ₂ H ₆)/ ν_{12} (C ₄ H ₁₀)/ ν_{23} (C ₄ H ₈)	Combination/CH ₂ asymmetric stretch	(5), (9), (11), (18)
...	2918	$\nu_8 + \nu_{11}$ (C ₂ H ₆)	Combination	(4), (5), (13)
...	2880	ν_5 (C ₂ H ₆)/ ν_{28} (C ₄ H ₁₀)	CH ₃ stretch	(4), (5), (9), (13)
...	2862	ν_{29} (C ₄ H ₁₀)	CH ₂ symmetric stretch	(4), (7), (13)
...	2832	$\nu_6 + \nu_{11}$ (C ₂ H ₆)	Combination	(5)
...	2740	$\nu_2 + \nu_6$ (C ₂ H ₆)	Combination	(4), (5)
...	2340	ν_6 (CO ₂)	CO asymmetric stretch	(3), (14)
2138	...	ν_1 (CO)	CO stretch	(3), (6), (14)
2090	...	ν_1 (¹³ CO)	CO stretch	(3), (6), (14)
2087	...	ν_1 (C ¹⁸ O)	CO stretch	(3), (14)
2043	...	ν_1 (¹³ C ¹⁸ O)	CO stretch	(14)
1965	...	$\nu_4 + \nu_8$ (C ₂ H ₄)	Combination	(5)
1899	...	$\nu_7 + \nu_8$ (C ₂ H ₄)	Combination	(5)
...	1845	ν_3 (HCO)	CO stretch	(6), (15)
...	1823	ν_2 (HOCO)/ ν_2 (c-C ₃ H ₄ O)	CO stretch	(15), (19)
...	1722	(a)	CO stretch	(6), (16), (17)
...	1696	(b)	CO stretch	(16)
...	1680	(c)	CO stretch	(16)
...	1642	ν_4 (C ₄ H ₈)	C=C stretch	(4), (9)
1619	...	ν_2 (C ₂ H ₄)	C=C stretch	(6), (7), (10)
...	1464	ν_{11} (C ₂ H ₆)/ $\nu_{14}, \nu_{30}, \nu_{31}$ (C ₄ H ₁₀)	CH ₃ bend	(4), (5), (9), (15)
1439	...	ν_{12} (C ₂ H ₄)	CH ₂ scissor	(2), (6), (7), (10)
...	1377	ν_6 (C ₂ H ₆)/ ν_{32} (C ₄ H ₁₀)	CH ₃ symmetric deformation	(5), (9), (12)
1339	...	ν_3 (C ₂ H ₄)	CH ₂ scissor	(6), (7), (10)
1224	...	ν_6 (C ₂ H ₄)	CH ₂ rock	(6), (7), (10)
953	...	ν_7 (C ₂ H ₄)	CH ₂ wag	(2), (6), (7), (8), (10)
823	...	ν_{10} (C ₂ H ₄)	CH ₂ rock	(6), (7), (10)
...	758	ν_5 (C ₂ H ₂)	CCH bend	(7), (20)

Notes. (a) RC(=O)H saturated aliphatic aldehydes. (b) R₁R₂C=CR₃–CH=O or RC≡C–CH=O α, β -unsaturated aldehydes (carbonyl) and R₁R₂C=CR₃–C(=O)R₄ (R₄ ≠ H) or R₁C≡C–C(=O)R₂ (R₂ ≠ H) α, β -unsaturated ketones (carbonyl). (c) R₁R₂C=CR₃–CH=O or RC≡C–CH=O α, β -unsaturated aldehydes (carbonyl) and R₁R₂C=CR₃–C(=O)R₄ (R₄ ≠ H) or R₁C≡C–C(=O)R₂ (R₂ ≠ H) α, β -unsaturated ketones (carbonyl), R₂C=CH₂ or RHC=CHR disubstituted (trans), R₂C=CHR trisubstituted, and R₂C=CR₂ tetrasubstituted alkenes.

References. (1) Brock et al. (1994), (2) Bohn et al. (1994), (3) Jamieson et al. (2006), (4) Zhou et al. (2014), (5) Ennis et al. (2011), (6) Bennett et al. (2005a), (7) Shimanouchi (1972), (8) Cowieson et al. (1981), (9) Kim et al. (2010), (10) Rytter & Gruen (1979), (11) Bennett et al. (2006), (12) Kaiser & Roessler (1998), (13) Comeford & Gould (1961), (14) Bennett et al. (2009), (15) Bennett & Kaiser (2007a), (16) Kaiser et al. (2014), (17) Bennett et al. (2005b), (18) Levin et al. (1973), (19) Breda et al. (2012), (20) Coustenis et al. (1999).

subliming molecules with 10.49 eV photons. Here, mass peaks beyond $m/z = 56$ (C₃H₄O⁺) are clearly visible. Corresponding isotopic shifts are observed in the C¹⁸O–C₂D₄ system (Figure 7(b)). Recall that by using a photoionization energy of 9.60 eV (Figure 7(c)), propenal cannot be ionized, but only the cyclopropanone isomer (9.10 eV). In the present paper, we only focus on the formation of propenal (C₂H₃HCO; 56 amu) and cyclopropanone (c-C₃H₄O; 56 amu) due to their astrochemical relevance and to highlight the capabilities of the new machine to discriminate and to detect both isomers. The complete product spectra are disseminated in a forthcoming publication.

Figure 8(a) displays the TPD profiles, i.e., the intensity of a well-defined ion count of the photoionized molecule versus the temperature at $m/z = 56$ from 60 to 300 K; no signal was monitored from 10 to 60 K. As visible from signal at $m/z = 56$ from 87 to 162 K, it is evident that molecules of $m/z = 56$ can be formed during the irradiation of carbon monoxide (CO)–ethylene (C₂H₄) ices. However, signal at $m/z = 56$ can be attributed to three molecules: propenal (C₃H₄O⁺; $m/z = 56$; IE = 10.10 eV), cyclopropanone (C₃H₄O⁺; $m/z = 56$; IE = 9.10 eV), and also butene (C₄H₈⁺; $m/z = 56$; IE = 9.55 eV). Since recent experiments in our group depicted that butene is one of the major products in the low temperature radiolysis of solid ethylene (Zhou et al. 2014), isotopically labeled ices

Table 2
Infrared Absorption Features Before and After the Irradiation of ^{18}O -Carbon monoxide— D_4 -Ethylene Ices ($\text{C}^{18}\text{O}-\text{C}_2\text{D}_4$) at 5.5 K

Absorptions Before Irradiation (cm^{-1})	Absorptions After Irradiation (cm^{-1})	Assignment	Carrier	References
4610, 4461, 4441, 4409, 3844, 3378, 3329, 3306, 3186	...	$\nu_9 + 2\nu_6, \nu_9 + \nu_2, \nu_{11} + \nu_2, \nu_5 + \nu_{12}, \nu_9 + \nu_3, \nu_9 + \nu_6, \nu_{11} + \nu_3, \nu_{11} + \nu_6$ (C_2D_4)	Overtone/ Combinations	(3), (21)
4147	...	$2\nu_1$ (C^{18}O)	Overtone	(14), (15)
...	2590	ν_3 (C_2D_2)	CD stretch	(4)
...	2406	ν_3 (C_2D_2)	CD stretch	(6), (7), (12)
2341	...	ν_3 (CO_2)	CO asymmetric stretch	(14)
2332	...	ν_9 (C_2D_4)	CD_2 asymmetric stretch	(7), (22)
2307	...	ν_3 (C^{18}O_2)	CO asymmetric stretch	(14), (15)
2249	...	ν_3 ($^{13}\text{C}^{18}\text{O}_2$)	CO asymmetric stretch	(14), (15)
...	2228	ν_7 (C_2D_6)/ ν_{23} (C_4D_8)	CD_3 degenerate stretch	(12), (18), (23)
...	2219	$\nu_2 + \nu_8$ (C_2D_6)	Combination	(23)
2192	...	ν_{11} (C_2D_4)	CD_2 symmetric stretch	(7), (22)
2137	...	ν_1 (CO)	CO stretch	(3)
2110	...	ν_1 (C^{17}O)	CO stretch	(14), (15)
2084	...	ν_1 (C^{18}O)	CO stretch	(14), (15)
2037	...	ν_1 ($^{13}\text{C}^{18}\text{O}$)	CO stretch	(14), (15)
...	1772	ν_3 (DC^{18}O)	CO stretch	(16)
...	1768	ν_2 (DOC^{18}O)	CO stretch	(15)
...	1674	(a)	CO stretch	(16)
...	1653	(b)	CO stretch	(16)
...	1643	(c)	CO stretch	(16)
1073	...	ν_{12} (C_2D_4)	CD_2 scissor	(7), (22)
723	...	ν_7 (C_2D_4)	CD_2 wag	(7), (8), (9), (10), (12), (22)

Notes. (a) $\text{RC}(=\text{O})\text{H}$ saturated aliphatic aldehydes. (b) $\text{R}_1\text{R}_2\text{C}=\text{CR}_3-\text{CH}=\text{O}$ or $\text{RC}\equiv\text{C}-\text{CH}=\text{O}$ α, β -unsaturated aldehydes (carbonyl) and $\text{R}_1\text{R}_2\text{C}=\text{CR}_3-\text{C}(=\text{O})\text{R}_4$ ($\text{R}_4 \neq \text{H}$) or $\text{R}_1\text{C}\equiv\text{C}-\text{C}(=\text{O})\text{R}_2$ ($\text{R}_2 \neq \text{H}$) α, β -unsaturated ketones (carbonyl). (c) $\text{R}_1\text{R}_2\text{C}=\text{CR}_3-\text{CH}=\text{O}$ or $\text{RC}\equiv\text{C}-\text{CH}=\text{O}$ α, β -unsaturated aldehydes (carbonyl) and $\text{R}_1\text{R}_2\text{C}=\text{CR}_3-\text{C}(=\text{O})\text{R}_4$ ($\text{R}_4 \neq \text{H}$) or $\text{R}_1\text{C}\equiv\text{C}-\text{C}(=\text{O})\text{R}_2$ ($\text{R}_2 \neq \text{H}$) α, β -unsaturated ketones (carbonyl), $\text{R}_2\text{C}=\text{CH}_2$ or $\text{RHC}=\text{CHR}$ disubstituted (trans), $\text{R}_2\text{C}=\text{CHR}$ trisubstituted, and $\text{R}_2\text{C}=\text{CR}_2$ tetrasubstituted alkenes.

References. (21) Gallaway & Barker (1942), (22) Dows (1962), (23) Tejada & Eggers (1976).

($\text{C}^{18}\text{O}-\text{C}_2\text{D}_4$) were used to separate the overlapping $\text{C}_3\text{H}_4\text{O}^+$ and C_4H_8^+ molecular ions.

Here, Figure 8(b) depicts the TPD profile of $m/z = 64$, i.e., D8-butene (C_4D_8^+) which is shifted by 8 amu due to the replacement of eight hydrogen atoms in butene (C_4H_8) by deuterium. Here, D8-butene sublimates at a temperature range from 90 to 129 K, which overlaps with the sublimation range of $m/z = 56$ for the carbon monoxide (CO)–ethylene (C_2H_4) ices. Since D8-butene is shifted by 8 amu, D8-butene (C_4D_8^+ ; $m/z = 64$) will not overlap with signal originating from $\text{C}_3\text{D}_4^{18}\text{O}^+$ ($m/z = 62$) in the irradiated $\text{C}^{18}\text{O}-\text{C}_2\text{D}_4$ system. Note that a dedicated calibration experiment was also carried out (Figure 8(c)) to demonstrate that upon irradiation D4-ethylene ice does not form any molecules and/or fragment ions upon ionization overlapping with $m/z = 62$ ($\text{C}_3\text{D}_4^{18}\text{O}^+$). Figure 8(d) presents the TPD spectrum recorded at $m/z = 62$ ($\text{C}_3\text{D}_4^{18}\text{O}^+$) depicting a signal from 96 to 173 K. However, since a photoionization energy of 10.49 eV was used, this signal could originate from the propenal isomer (IE = 10.10 eV) and/or the cyclopropanone isomer (IE = 9.10 eV). It is worth mentioning that two distinct peaks are observable (Figure 8(d)), which could indicate that both isomers are formed.

Next, by focusing on the $\text{C}^{18}\text{O}-\text{C}_2\text{D}_4$ system there will be no overlapping mass-to-charge peaks corresponding to hydrocarbons and will only produce a mass-to-charge signal corresponding to a $\text{C}_3\text{D}_4^{18}\text{O}^+$ ion $m/z = 62$. Also, tuning of the photoionization energy to 9.60 eV, which is below the ionization energy of propenal (IE = 10.10 eV) but above

the ionization energy of the cyclopropanone isomer (IE = 9.10 eV), allows for isomer specific discrimination as only the cyclopropanone isomer can be ionized and therefore detected at $m/z = 62$. Indeed, Figure 8(e) depicts clearly the presence of a molecular ion corresponding to $m/z = 62$ ($\text{C}_3\text{D}_4^{18}\text{O}^+$) from 90 to 133 K; this indicates that cyclopropanone ($\text{c}-\text{C}_3\text{D}_4^{18}\text{O}$) must be formed in the experiments. A detailed comparison of data taken at 10.49 and 9.60 eV also exhibits a pronounced peak from 123 to 173 K in the 10.49 eV experiment, which can only origin from the propenal isomer. Therefore, both the propenal and the cyclopropanone isomers are formed in the experiments with propenal and cyclopropanone subliming from 123 K to 173 K and 90 K to 133 K, respectively, as reflected in the enhanced polarity of propenal compared to the cyclopropanone isomer.

Additional calibration experiments were conducted to verify our conclusions. Here, we prepared carbon monoxide–ethylene ices doped with 1% butene isomers as well as propenal and conducted TPD studies with a photoionization energy of 10.49 eV (Figure 9(a)) with the aim to compare the sublimation temperature of the dopants with the actual experimental data of the electron irradiated samples. Figure 9(b) presents the scaled TPD profiles of the subliming propenal dopants overlapped with the data recorded at $m/z = 62$ in the irradiated $\text{C}^{18}\text{O}-\text{C}_2\text{D}_4$ system. However, this overlap of the two signals shows that the determination of which isomer belongs to which peak of $m/z = 62$ is ambiguous based on the calibration experiments alone.

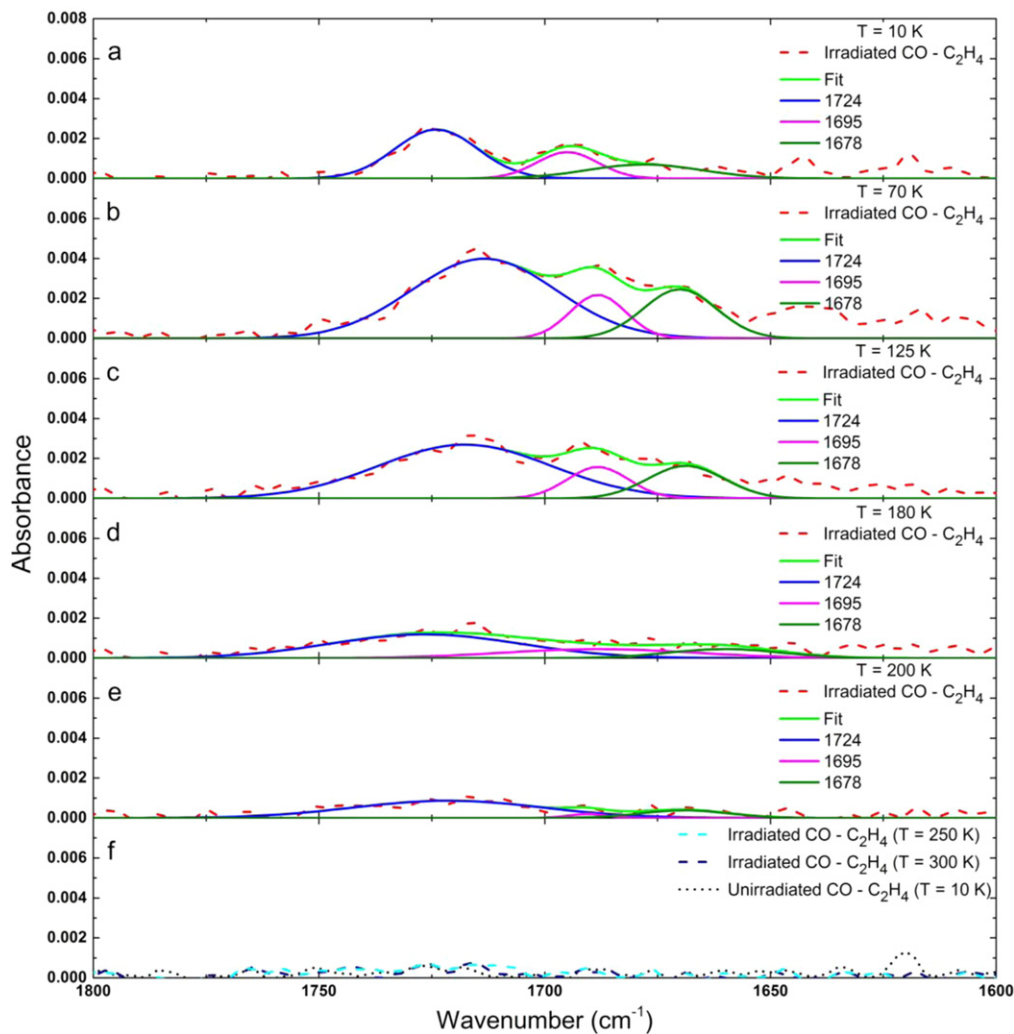


Figure 6. Deconvolutions of the infrared spectra in the carbonyl region of the carbon monoxide–ethylene ice during warm up at several temperatures with the deconvoluted peak center positions labeled: (a) 10 K (after irradiation) (b) 70 K (before $m/z = 56$ is detected by ReTOF) (c) 125 K (temperature at trough between $m/z = 56$ peaks; see Figure 8(d)) (d) 180 K (after $m/z = 56$ is no longer detected by ReTOF; infrared carbonyl band still present) (e) 200 K (after $m/z = 56$ is no longer detected by ReTOF; infrared carbonyl band still present) (f) infrared spectra of the 10 K unirradiated CO–C₂H₄ ice, the irradiated ice at 250 K, and the irradiated ice at 300 K (infrared carbonyl band is not detectable).

Therefore, a tunable ionization experiment was necessary to definitively distinguish if the $m/z = 62$ was from a single isomer or from multiple isomers (Figure 9(c)). Figure 9(d) shows an overlay of the $m/z = 62$ cyclopropanone peak with the 1% propenal calibration which still shows some overlapping of the two peaks, but an offset in the sublimation onset temperature of 20 K. Comparison of the 1% propenal calibration experiment to the $m/z = 62$ propenal peak is accomplished by subtracting the $m/z = 62$ peak belonging only to cyclopropanone from the entire peak of $m/z = 62$ at 10.49 eV, which could be either isomer, shows a distinct separate peak belonging to propenal (Figure 9(e)). Figure 9(f) displays the TPD overlay of the subliming propenal dopants with the $m/z = 62$ due to propenal, after subtraction of cyclopropanone, and this shows a concurrent onset sublimation temperature of 109 K substantiating that this peak is due to the propenal isomer.

In summary, exploiting PI-ReTOF-MS we have provided compelling evidence that both the propenal (C₃H₄O) and cyclopropanone (c-C₃H₄O) isomers are formed during the irradiation of carbon monoxide–ethylene ices. Further, utilizing absolute photoionization cross sections of 6.80 ± 1.36 Mb and

25 ± 5 Mb (Adam & Zimmermann 2007; Goulay et al. 2012) for propenal and cyclopropanone, respectively, a relative abundance of $(4.5 \pm 0.9):1.0$ of propenal (C₃H₄O) versus cyclopropanone (c-C₃H₄O) was determined via PI-ReTOF-MS. Thus, propenal is formed predominantly.

4.3. Quantitative and Correlation of FT-IR and PI-ReTOF-MS

Since both C₃H₄O isomers were detected using PI-ReTOF-MS, these data can be correlated with the FTIR data that were initially ambiguous as to what exact isomers were formed. Recall that a calibration experiment using a 1% mixture of the propenal isomer in carbon monoxide and ethylene was deposited at 5.5 K and then sublimed while monitored with the ReTOF instrument. The FTIR signal of the 1% calibration experiment corresponds to a column density of $3.2 \pm 0.9 \times 10^{15}$ to $6.3 \pm 1.8 \times 10^{15}$ molecules cm⁻² using an experimentally derived absorption coefficient of 2.46×10^{-17} cm molecules⁻¹ which lies within calculated intensities of 2.44×10^{-17} , 3.47×10^{-17} , and 4.67×10^{-17} cm molecules⁻¹ (Xu et al. 2011; Puzzarini et al. 2014). This calibration experiment allows for the calculation of the unknown abundance of each

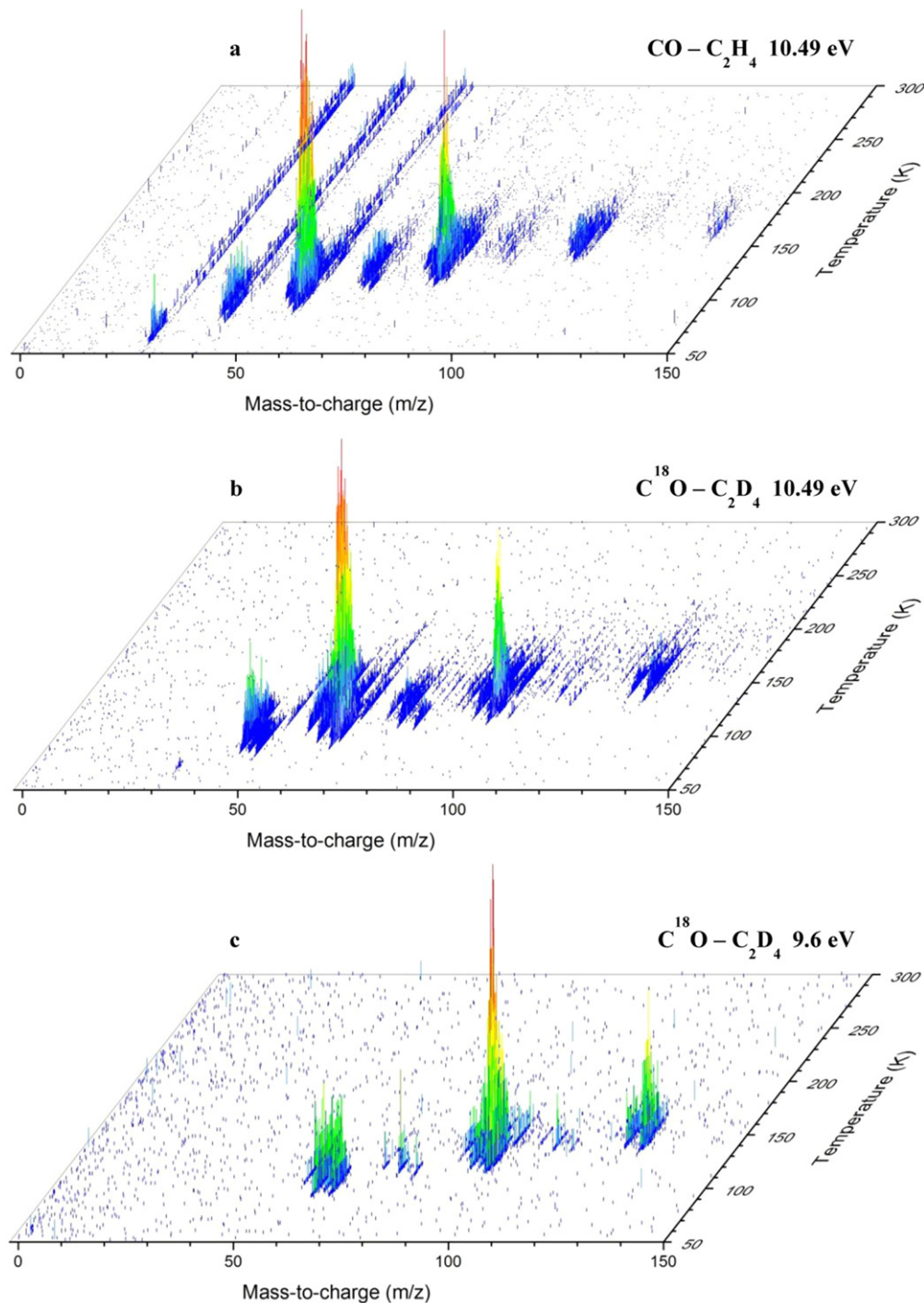


Figure 7. (a) PI-ReTOF-MS (PI = 10.49 eV) data as a function of temperature of the newly formed products subliming into the gas phase from the irradiated carbon monoxide–ethylene ices ($\text{CO-C}_2\text{H}_4$). (b) PI-ReTOF-MS (PI = 10.49 eV) data as a function of temperature of the newly formed products subliming into the gas phase from the irradiated ^{18}O -carbon monoxide– D_4 -ethylene ices ($\text{C}^{18}\text{O-C}_2\text{D}_4$). (c) PI-ReTOF-MS (PI = 9.60 eV) data as a function of temperature of the newly formed products subliming into the gas phase from the irradiated ^{18}O -carbon monoxide– D_4 -ethylene ices ($\text{C}^{18}\text{O-C}_2\text{D}_4$). The max intensity of each plot was scaled to 100%.

isomer in the irradiated ice. The PI-ReTOF-MS integrated signal for the 1% propenal calibration experiment is 19.5 ± 1.4 times larger than the signal produced from the irradiated ice for propenal ($m/z = 62$) signal (Figure 9(e)) suggesting column densities of formed propenal molecules of $1.1 \pm 0.3 \times 10^{14}$ to $2.0 \pm 0.6 \times 10^{14}$ molecules cm^{-2} .

Furthermore, the ratio discussed above of $(4.5 \pm 0.9):1.0$ of propenal to cyclopropanone can also be applied, utilizing

calculated infrared intensities for cyclopropanone’s carbonyl stretching of 5.41×10^{-17} , 6.21×10^{-17} , 6.47×10^{-17} , and 7.11×10^{-17} $\text{cm}^2 \text{molecules}^{-1}$ (Corkran & Ball 2004; Breda et al. 2012), results in cyclopropanone column densities between $3.2 \pm 0.9 \times 10^{13}$ and $4.2 \pm 1.2 \times 10^{13}$ molecules cm^{-2} . As stated earlier the FTIR bands that correspond to these isomers were contaminated by the possibility of having overlapping bands from other molecules present in the

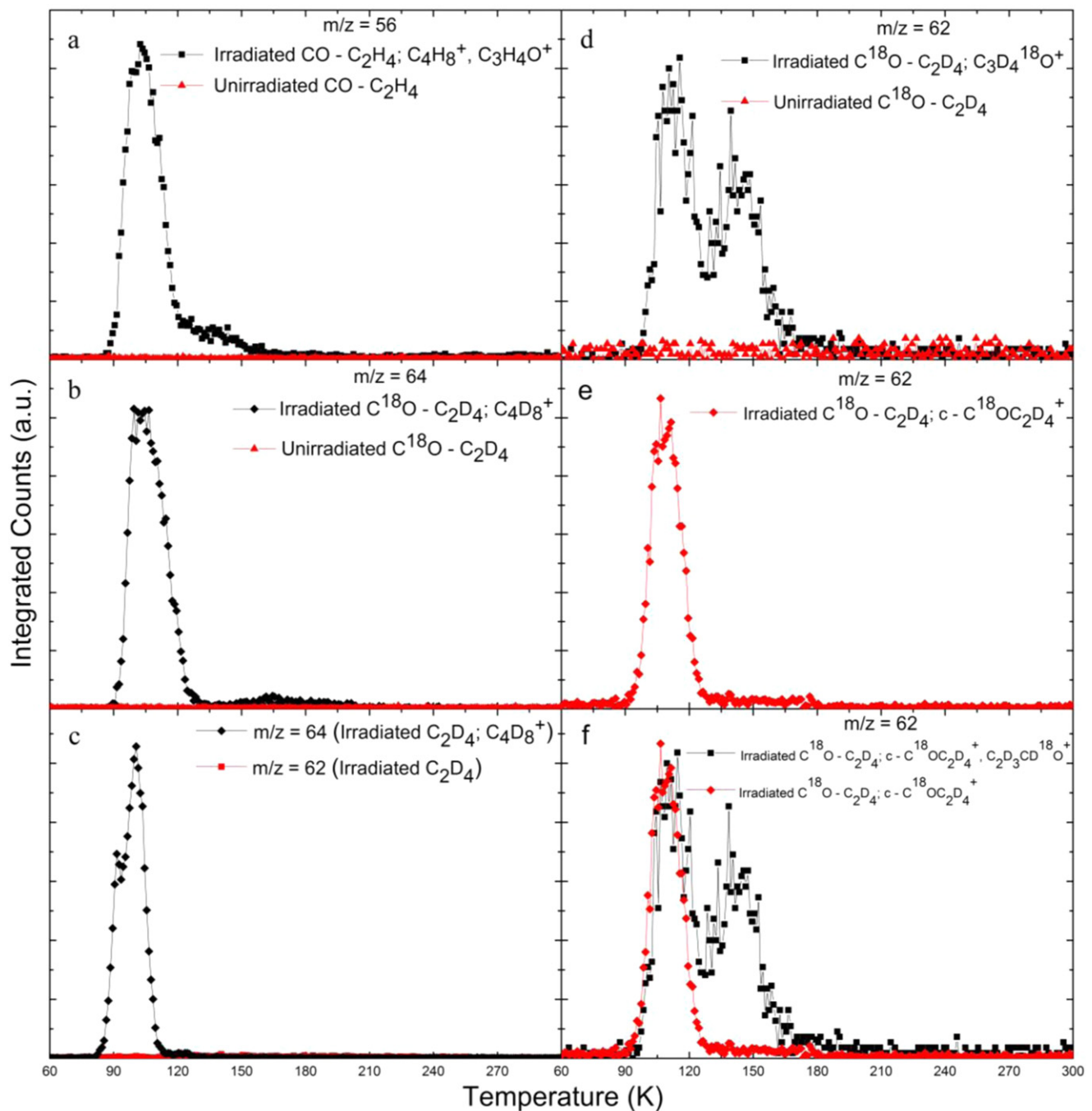


Figure 8. (a) Sublimation profiles of the ion counts at $m/z = 56$ ($C_4H_8^+$, $C_3H_4O^+$) recorded with PI-ReTOF-MS (PI = 10.49 eV, black—irradiated ice, red—unirradiated ice) for the CO-C₂H₄ system. (b) Sublimation profiles of the ion counts at $m/z = 64$ ($C_4D_8^+$) recorded with PI-ReTOF-MS (PI = 10.49 eV, black—irradiated ice, red—unirradiated ice) for the C¹⁸O-C₂D₄ system. (c) Sublimation profiles of the ion counts at $m/z = 64$ ($C_4D_8^+$) and $m/z = 62$ recorded with PI-ReTOF-MS (PI = 10.49 eV, black— $m/z = 64$, red— $m/z = 62$) for the irradiated C₂D₄ system. (d) Sublimation profiles of the ion counts at $m/z = 62$ ($C_3D_4^{18}O^+$) recorded with PI-ReTOF-MS (PI = 10.49 eV, black—irradiated ice, red—unirradiated ice) for the C¹⁸O-C₂D₄ system. Two peaks can be observed, which may correspond to both $C_3D_4^{18}O^+$ isomers ($C_2D_3CD^{18}O^+$, $c-C^{18}OC_2D_4^+$). (e) Sublimation profile of $m/z = 62$ ($c-C^{18}OC_2D_4^+$; I.E. = 9.1 eV) recorded by PI-ReTOF-MS (PI = 9.6 eV) from the irradiated C¹⁸O-C₂D₄ ice. (f) Overlay of PI-ReTOF-MS (PI = 10.49 eV) sublimation profiles for $m/z = 62$ ($c-C^{18}OC_2D_4^+$; I.E. = 9.1 eV) and $m/z = 62$ ($C_3H_4O^+$ isomers) from the irradiated C¹⁸O-C₂D₄ ice.

irradiated ice. However, the abundances obtained via PI-ReTOF-MS can now be correlated with the experimentally obtained FTIR bands before and after sublimation of the isomers to determine to what extent the FTIR bands correspond to these isomers.

The average column densities derived from the PI-ReTOF-MS data for propenal and cyclopropanone are $1.6 \pm 0.5 \times 10^{14}$

and $3.6 \pm 0.4 \times 10^{13}$ molecules cm^{-2} , respectively. Using the infrared bands of propenal (1696 cm^{-1}) and cyclopropanone (1822 cm^{-1}) average column densities of the isomers are $8.5 \pm 2.5 \times 10^{14}$ and $9.2 \pm 1.1 \times 10^{13}$ molecules cm^{-2} , respectively. However, these column densities have overlapping bands from other complex molecules such as α , β —unsaturated aldehydes (1696 cm^{-1}) or the hydroxycarbonyl radical

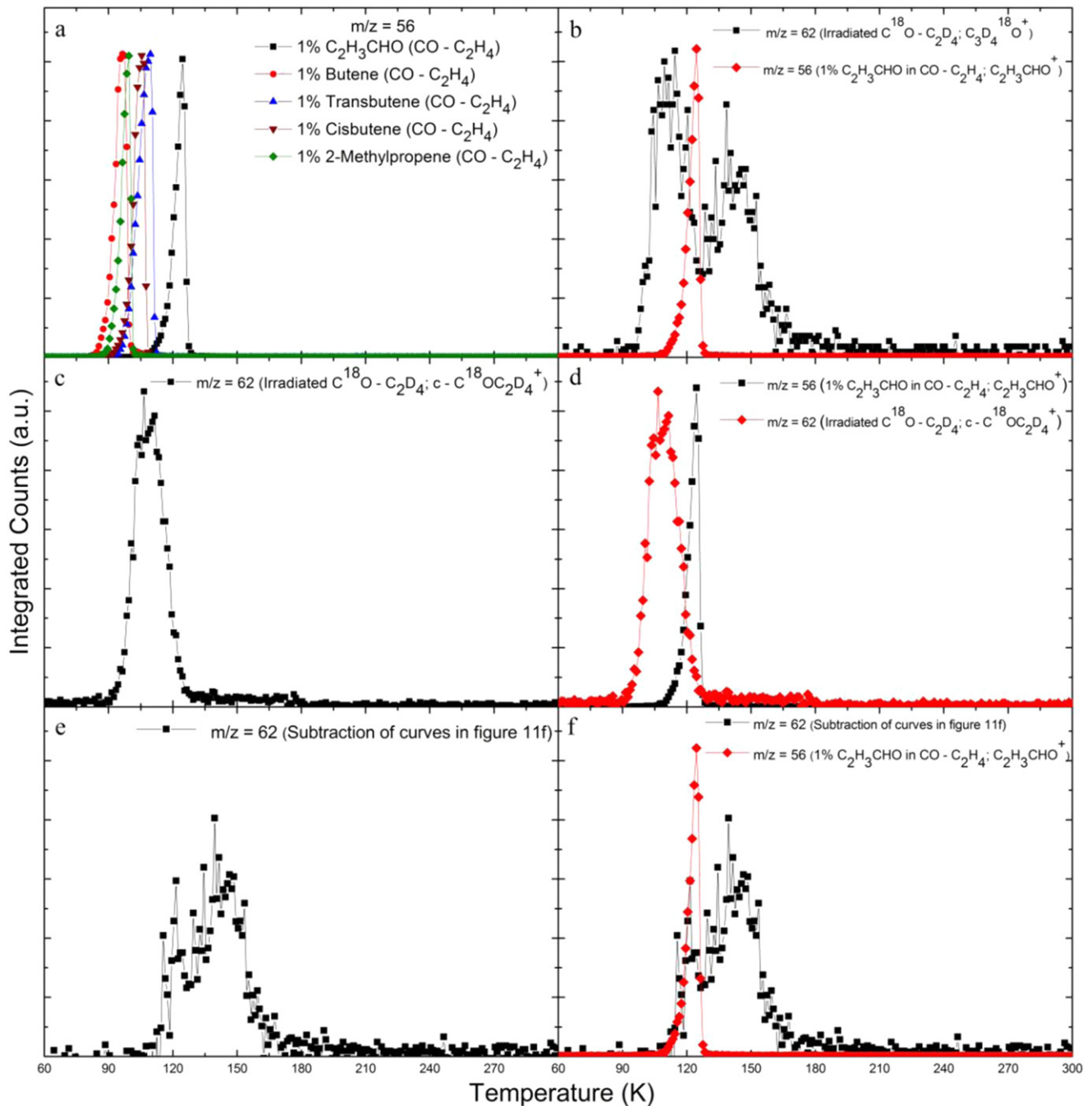


Figure 9. (a) Calibration experiments PI-ReTOF-MS (PI = 10.49 eV) of 1% propenal ($\text{C}_2\text{H}_3\text{CHO}^+$; $m/z = 56$; 10.1 eV) and 1% C_4H_8 isomers (butene, transbutene, cisbutene, and 2-methylpropene; $m/z = 56$; I.E. = 9.1–9.6 eV) in $\text{CO}-\text{C}_2\text{H}_4$ ice. (b) Overlay of PI-ReTOF-MS (PI = 10.49 eV) sublimation profiles for 1% propenal ($\text{C}_2\text{H}_3\text{CHO}^+$; $m/z = 56$; I.E. = 10.1 eV; red) and $m/z = 62$ ($\text{C}_3\text{H}_4\text{O}^+$ isomers; black) from the irradiated $\text{C}^{18}\text{O}-\text{C}_2\text{D}_4$ ice. (c) Sublimation profile of $m/z = 62$ ($\text{c}-\text{C}^{18}\text{OC}_2\text{D}_4^+$ (C_2D_4^+ ; I.E. = 9.1 eV) recorded by PI-ReTOF-MS (PI = 9.6 eV) from the irradiated $\text{C}^{18}\text{O}-\text{C}_2\text{D}_4$ ice. (d) Overlay of PI-ReTOF-MS (PI = 10.49 eV) sublimation profiles for 1% propenal ($\text{C}_2\text{H}_3\text{CHO}^+$; $m/z = 56$) and $m/z = 62$ ($\text{c}-\text{C}^{18}\text{OC}_2\text{D}_4^+$) from the irradiated $\text{C}^{18}\text{O}-\text{C}_2\text{D}_4$ ice. (e) Result of subtraction of $m/z = 62$ ($\text{c}-\text{C}^{18}\text{OC}_2\text{D}_4^+$) from $m/z = 62$ ($\text{C}_3\text{H}_4\text{O}^+$ isomers) in Figure 8(f) to produce a peak relating only to propenal ($\text{C}_2\text{D}_3\text{CD}^{18}\text{O}^+$; $m/z = 62$; 10.1 eV). (f) Overlay of PI-ReTOF-MS (PI = 10.49 eV) sublimation profiles for 1% propenal ($\text{C}_2\text{H}_3\text{CHO}^+$; $m/z = 56$) and the subtraction peak (12e) corresponding to propenal $m/z = 62$ ($\text{C}_2\text{D}_3\text{CD}^{18}\text{O}^+$).

(1822 cm^{-1}) and it was necessary to deconvolute the propenal (1696 cm^{-1}) band from other closely related carbonyl containing complex molecules. Therefore, these abundances represent the limiting case of what could possibly be present in the irradiated ice for each isomer if the assumption is made that there were no other overlapping bands. However, these abundances derived from the FTIR can be further bounded by subtracting interfering species from the infrared band of interest.

During the TPD studies the ice is monitored while the subliming molecules are concurrently monitored in the gas phase. By monitoring the change of the infrared bands as the sample is heated while also monitoring when the isomers sublime it is possible to determine what portion of the initial post irradiation infrared band is due to the isomer of interest. The average column densities derived from this method using the FTIR bands of propenal (1696 cm^{-1}) and cyclopropanone

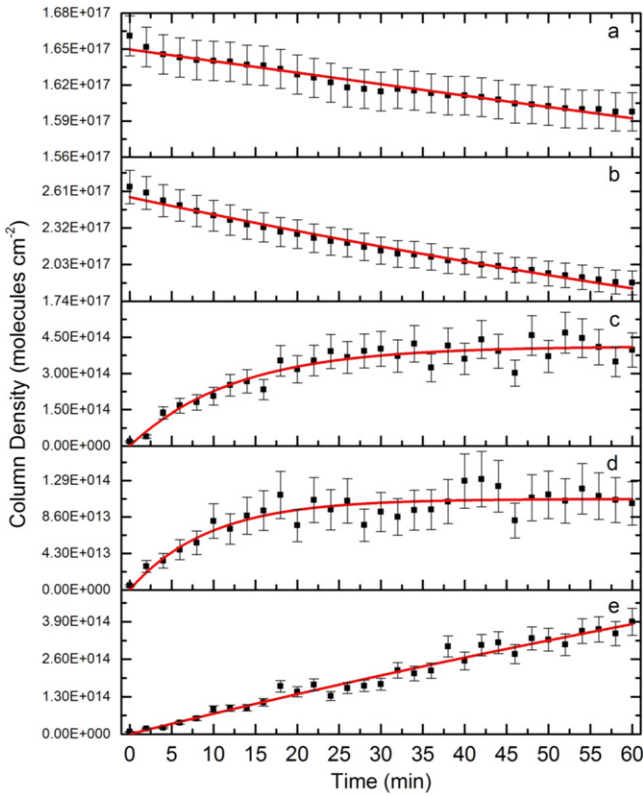


Figure 10. Temporal evolution and kinetic fitting of (a) carbon monoxide (CO) at 2136 cm^{-1} . (b) Ethylene (C_2H_4) at 1439 cm^{-1} . (c) Formyl radical (HCO) at 1845 cm^{-1} . (d) Cyclopropanone ($\text{c-C}_3\text{H}_4\text{O}$)/hydroxycarbonyl radical (HOCO) at 1822 cm^{-1} . (e) Propenal ($\text{C}_2\text{H}_3\text{CHO}$)/unsaturated aldehydes at 1696 cm^{-1} .

(1822 cm^{-1}) average column densities of the isomers were corrected to $2.0 \pm 0.2 \times 10^{14}$ and $4.5 \pm 0.5 \times 10^{13}$ molecules cm^{-2} , respectively. These abundances are within the error limits of the abundances derived from the PI-ReTOF-MS data. Also, the ratio of propenal to cyclopropanone from the PI-ReTOF-MS, FT-IR raw data, and corrected FT-IR data are $(4.5 \pm 0.9):1$, $(9.3 \pm 3.7):1$, and $(4.5 \pm 0.9):1$, respectively. Note that the corrected FTIR data shows an identical ratio to the relative abundance derived from the PI-ReTOF-MS data. This correlation reflects that the subtraction of interfering species from the infrared bands represents an elegant approach to determine abundances of complex molecules using infrared data, but only when coupled to a much more sensitive technique, such as PI-ReTOF-MS.

Also, by monitoring the evolution of each of these species during irradiation the percentage of the starting materials that are incorporated into the newly formed molecules can be calculated (Figure 10). If the infrared bands of the isomers are assumed to be entirely propenal or cyclopropanone, then $6 \pm 2\%$ and $2 \pm 1\%$ of the destroyed carbon monoxide is used to form these isomers, respectively. Also, of the destroyed ethylene molecules $0.5 \pm 0.2\%$ and $0.13 \pm 0.04\%$ form propenal and cyclopropanone, respectively. Furthermore, the average energy deposited by the electrons used to process the ice was calculated to be 3.7 keV ; therefore the yield of each molecule per electron volt absorbed energy produced from the irradiation can be calculated. Utilizing the corrected infrared column densities, where interfering species were subtracted, for propenal and cyclopropanone values of $8.0 \pm 0.9 \times 10^{-5}$

Table 3

Reaction Pathways and Derived Rate Constants to Fit the Temporal Evolution of the $\text{C}_3\text{H}_4\text{O}$ Isomers in the Irradiated Ethylene–Carbon Monoxide Ice

Reactions		Rate Constants
$\text{CO} \rightarrow \text{X}$	k_1	$(5.9 \pm 0.2) \times 10^{-4}$
$\text{C}_2\text{H}_4 \rightarrow \text{C}_2\text{H}_3 + \text{H}$	k_2	$(5.5 \pm 0.1) \times 10^{-3}$
$\text{H} + \text{CO} \rightarrow \text{HCO}$	k_3	$(7.9 \pm 0.9) \times 10^{-2}$
$\text{HCO} + \text{C}_2\text{H}_3 \rightarrow \text{C}_2\text{H}_3\text{CHO}$	k_4	$(4 \pm 3) \times 10^{-3}$
$\text{CO} + \text{C}_2\text{H}_4 \rightarrow \text{c-C}_3\text{H}_4\text{O}$	k_5	$(1.1 \pm 0.2) \times 10^{-1}$

Note. Units: k_1 – k_5 are in s^{-1} (first order).

molecules eV^{-1} and $1.8 \pm 0.2 \times 10^{-5}$ molecules eV^{-1} , respectively, can be obtained.

5. DISCUSSION

Having identified the propenal ($\text{C}_2\text{H}_3\text{CHO}$) and cyclopropanone ($\text{c-C}_3\text{H}_4\text{O}$) molecules in electron irradiated carbon monoxide–ethylene ices at 5.5 K , the temporal evolution of both isomers as well as the formyl radical (HCO) and the starting materials carbon monoxide (CO) and ethylene (C_2H_4) can be obtained and kinetically fit (Figure 10; Table 3). Best fits were achieved by fitting the experimentally obtained carbon monoxide and ethylene column densities via first-order decay upon electron bombardment (Equations (1)–(4)).

$$-d[\text{CO}]/dt = k_1[\text{CO}], \quad (1)$$

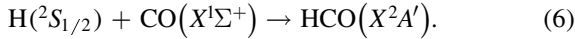
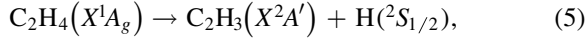
$$-d[\text{C}_2\text{H}_4]/dt = k_2[\text{C}_2\text{H}_4], \quad (2)$$

$$[\text{CO}](t) = [\text{CO}](t=0)e^{-k_1 t}, \quad (3)$$

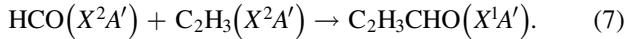
$$[\text{C}_2\text{H}_4](t) = [\text{C}_2\text{H}_4](t=0)e^{-k_2 t}. \quad (4)$$

The best fit of the carbon monoxide column density (Figure 10(a)) profile using $[\text{CO}](t=0) = 1.65 \pm 0.01 \times 10^{17}$ molecules cm^{-2} yielded $k_1 = 5.9 \pm 0.2 \times 10^{-4}\text{ s}^{-1}$. Also, the best fit of the ethylene column density (Figure 10(b)) profile using $[\text{C}_2\text{H}_4](t=0) = 2.56 \pm 0.01 \times 10^{17}$ molecules cm^{-2} resulted in $k_2 = 5.5 \pm 0.1 \times 10^{-3}\text{ s}^{-1}$. The destruction of the initial ethylene and carbon monoxide molecules can result in the production of more complex molecules such as the $\text{C}_3\text{H}_4\text{O}$ isomers propenal ($\text{C}_2\text{H}_3\text{CHO}$) and cyclopropanone ($\text{c-C}_3\text{H}_4\text{O}$). A sensible reaction mechanism for the production of propenal is depicted via Equations (5)–(7) The initial step (Equation (5)) involves a carbon–hydrogen bond cleavage which is endoergic by 454 kJ mol^{-1} (4.7 eV) (Gurvich 1989). The calculated average energy implanted by the 5 keV electrons in the irradiated carbon monoxide–ethylene ice was $4.9 \pm 0.9\text{ eV}$ per C_2H_4 molecule on average showing that enough energy can be supplied to allow the carbon–hydrogen bond cleavage of ethylene to proceed. The released hydrogen atoms can have excess energy in form of translational energy (Kaiser & Roessler 1997; Bennett et al. 2005a). These can add via reaction (6) to the carbon monoxide molecule forming the formyl (HCO) radical; this process is exoergic (-58.6 kJ mol^{-1} , -0.60 eV), but has an entrance barrier of 8.3 kJ mol^{-1} (0.09 eV) (Wang et al. 1973; Werner et al. 1995), which can be easily overcome by the suprathreshold hydrogen

atom (Morton & Kaiser 2003).



If an ethylene molecule is neighboring a carbon monoxide molecule, a complex can exist in the ice [CO–C₂H₄]; then the carbon–hydrogen bond cleavage in ethylene followed by addition of the hydrogen atom to carbon monoxide can result in the formation of the formyl radical (HCO) and the vinyl radical (C₂H₃); in a barrierless recombination of these two radicals (reaction (7)), propenal (C₂H₃CHO) can be formed. The formation of propenal via reaction (7) is exoergic (–1.82 kJ mol^{–1}, –0.02 eV) (Gurvich 1989; Frenkel 1994; Simoes et al. 1996). If the formyl radical and the vinyl radical do not have a favorable geometry in the ice for recombination, then the formyl radical does not react to form propenal.

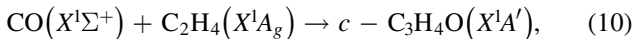


Overall, this would result in pseudo-first order profiles of the formyl radical (Figure 10(c)) and of propenal (Figure 10(e)):

$$[\text{HCO}](t) = a(1 - e^{-k_3 t}), \quad (8)$$

$$[\text{C}_2\text{H}_3\text{CHO}](t) = b(1 - e^{-k_4 t}). \quad (9)$$

Using Equation (8) to fit the formyl radical experimental data determines $k_3 = 7.9 \pm 0.9 \times 10^{-2} \text{ s}^{-1}$ and $a = 4.1 \pm 0.1 \times 10^{14} \text{ molecules cm}^{-2}$. Equation (9) was used to fit the propenal experimental data and yields $k_4 = 4 \pm 3 \times 10^{-3} \text{ s}^{-1}$ and $b = 1.6 \pm 0.9 \times 10^{15} \text{ molecules cm}^{-2}$. Overall, the formation of propenal from the reactants is exoergic by –21.2 kJ mol^{–1} (–0.22 eV) (Cox et al. 1989; Gurvich 1989; Frenkel 1994) (Equation (12)), $\text{CO}(X^1\Sigma^+) + \text{C}_2\text{H}_4(X^1A_g) \rightarrow \text{C}_2\text{H}_3\text{CHO}(X^1A')$. Finally, we discuss potential pathways to cyclopropanone (c-C₃H₄O). Here, the synthesis of cyclopropanone (c-C₃H₄O) by the addition of a single carbon monoxide molecule to the carbon–carbon ethylene double bond is feasible (reaction (10)), depending on the geometry of the molecules within the matrix. The formation of cyclopropanone,

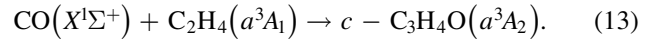
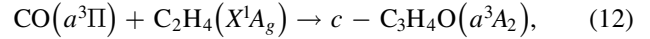


holds an endoergicity of 68.8 kJ mol^{–1} (0.71 eV) (Rodriguez et al. 1976; Cox et al. 1989; Gurvich 1989). The experimental data (Figure 10(d)) can be fit via pseudo-first order reaction with $k_5 = 1.1 \pm 0.2 \times 10^{-1} \text{ s}^{-1}$ and $c = 1.07 \pm 0.03 \times 10^{14} \text{ molecules cm}^{-2}$.

$$[c - \text{C}_3\text{H}_4\text{O}](t) = c(1 - e^{-k_5 t}). \quad (11)$$

It should be stressed that the reaction of singlet carbon monoxide with singlet ethylene—two closed shell molecules—holds a significant entrance barrier. Therefore, thermal carbon monoxide ($X^1\Sigma^+$) and ground state ethylene (X^1A_g) cannot form cyclopropanone. However, the reaction of excited state carbon monoxide ($a^3\Pi$) or ethylene (a^3A_1) with the co-reactants in their ground electronic states can result in the formation of the excited triplet products via barrier-less addition of the triplet reactants to the carbon–carbon double

bond of ethylene:



Here, the first excited triplet states of carbon monoxide and ethylene are 582.8 kJ mol^{–1} (6.04 eV) and 287.9 kJ mol^{–1} (2.98 eV) above their electronic ground state (Cooper & Langhoff 1981; Nguyen et al. 2008). The excitation energy can be supplied by the energy of the energetic electrons, which is significantly larger (5 keV) compared to the excitation energies of 6.04 and 2.98 eV.

6. ASTROPHYSICAL IMPLICATIONS

Within the astrophysical context of the processing of non-polar astrophysically relevant ices in the ISM, it is interesting to compare the rate constants and overall energetics of propenal ($k_4 = 4 \pm 3 \times 10^{-3} \text{ s}^{-1}$; –0.22 eV) with cyclopropanone formation ($k_5 = 1.1 \pm 0.2 \times 10^{-1} \text{ s}^{-1}$; +0.71 eV). Here, the formation of the thermodynamically less stable cyclopropanone isomer is actually *faster* than the synthesis of the energetically preferred isomer propenal by a factor of about 30. This finding can only be explained by a reaction mechanism—as extracted above—involving a non-equilibrium chemistry induced by the energetic electrons interacting with carbon monoxide and ethylene. Second, the faster rate constant could be the effect of a sterically less hindered pathway via a rapid, one step addition of electronically excited carbon monoxide to ethylene (or vice versa) compared to a pathway which may require unfavorable recombination geometries of two doublet radicals (formyl; vinyl) with their radical centers located at the carbon atoms. Here, propenal can be formed via radical–radical reaction during the irradiation within the ice as detected at 5.5 K and to a minor amount during the heating phase when the radicals stored in the matrix become mobile. On the other hand, cyclopropanone requires the reaction of triplet carbon monoxide and/or ethylene. These electronically excited molecules have short life times of $3.64 \pm 0.17 \times 10^{-3}$ and $10 \times 10^{-9} \text{ s}$ and hence cannot be “stored” within the ice matrix (Caldwell & Cao 1982; Jongma et al. 1997). Therefore, the formation of cyclopropanone via excited state triplet reactants must be correlated via a rapid reaction at 5.5 K under non-equilibrium conditions, but *not* via a thermal chemistry during the annealing phase of the ices. Therefore, the cyclopropanone molecule can be classified as a tracer of a low temperature non-equilibrium chemistry within interstellar ices, whereas propenal can be formed at 5.5 K and also during the annealing phase via non-equilibrium as well as thermal chemistry (radical recombination).

While carbon monoxide is a known constituent of ice coated interstellar grains (Strazzulla & Johnson 1991; Moore et al. 2001), the ethylene (C₂H₄) molecule has not been detected. However, ethylene has been shown in laboratory experiments to be formed easily in irradiated methane (CH₄) ices (Bennett et al. 2006). Based on our studies we can predict that the processing of the ice mantle of interstellar grains by galactic cosmic rays, which will generate secondary electrons within the ices can lead to the formation of both propenal and cyclopropanone in ices in cold molecular clouds. If these molecules are solely formed from ethylene and carbon monoxide, we can predict a ratio of formation and hence

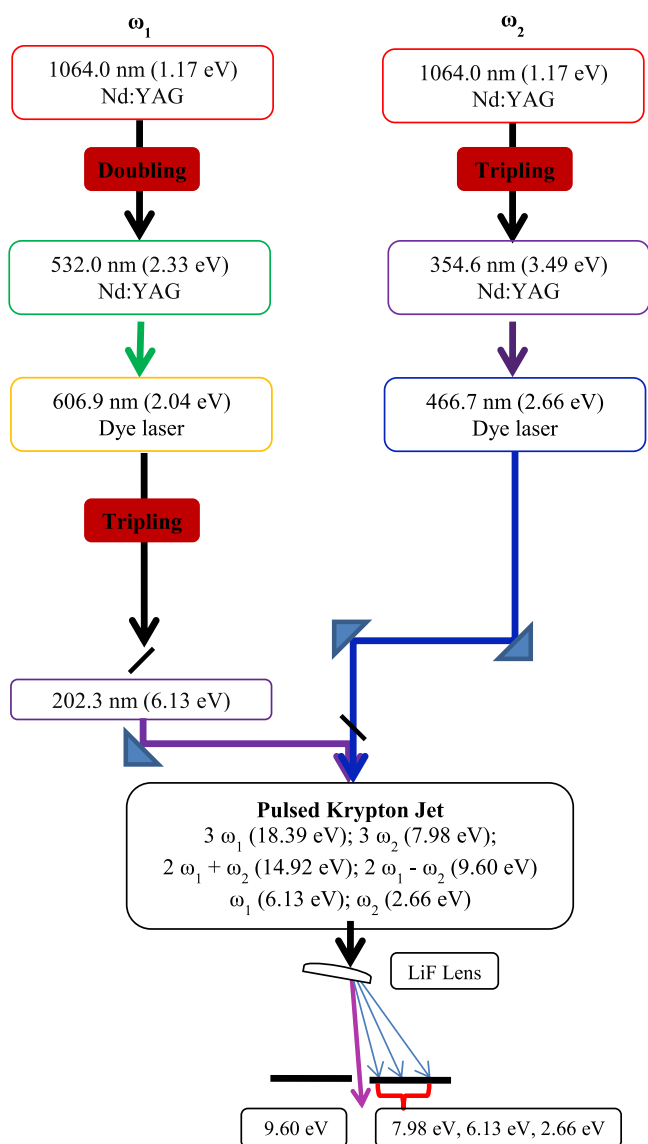


Figure 11. Flow diagram depicting the necessary wavelengths and optical components for the generation of coherent tunable vacuum ultraviolet light at 129.15 nm (9.60 eV) using resonant four-wave mixing.

release into the gas phase of about $(4.5 \pm 0.9):1$ of propenal versus cyclopropanone based on our infrared and reflectron time of flight data. Future experiments should be conducted by adding water to the ices to determine the effect of polar ices on the production of these isomers. These newly formed molecules within the ice can then be released into the gas phase as the molecular cloud transitions into a star-forming region such as Sgr B2(N).

Figure 1 shows two pairs of isomers, while both C_3H_2O isomers, propynal and cyclopropanone, have been detected in the ISM (Irvine et al. 1988; Hollis et al. 2006) the propenal isomer is the only C_3H_4O isomer that has been observed (Hollis et al. 2004). Therefore, future astronomical observations may wish to include both isomers in the survey as these experiments suggest that cyclopropanone can be formed on icy grains and should be in a relative abundance of about $(4.5 \pm 0.9):1$ (propenal to cyclopropanone). Applying the ratio measured in our experiments to the observed abundance of propenal

suggests that cyclopropanone should have a fractional abundance of approximately 1.6×10^{-9} , 7.5×10^{-11} , 5.8×10^{-10} , and 2.3×10^{-10} for NGC 7129-FIRS2, G-0.02, G-0.11, and G+0.693, respectively. Also, the ability to detect the cyclopropanone isomer will depend on its dipole moment as it will most likely be searched for using microwave spectroscopy, possibly using the Atacama Large Millimeter Array. The dipole of cyclopropanone is 2.67 D (Pochan et al. 1968), while propenal has a dipole of 3.05 D (Hollis et al. 2004). Comparing these values to the already detected isomers of propynal and cyclopropanone which have dipoles of 2.36 D and 4.39 D (Hollis et al. 2006), respectively, shows that the missing cyclopropanone isomer should have a strong enough dipole to be detected if it has the above approximated fractional abundances.

In summary, PI-ReTOF-MS-PI coupled with tunable photoionization has been established as a valuable tool to predict quantitatively the formation pathways and yields of structural isomers of COMs, which cannot be extracted with more traditional analytical tools such as FTIR and QMS. This data shows that novel techniques are now needed to confidently assign detections in laboratory ice analog experiments as the molecules of interest become more complex. Specifically, the propenal—cyclopropanone isomer pair can serve as a benchmark system to untangle not only non-equilibrium versus thermal reaction pathways, but also defines cyclopropanone as a tracer of low temperature non-equilibrium chemistry within interstellar ices. The prospective detection of even more COMs continues to grow in the ISM, and laboratory experiments will need to continue to improve to keep providing relevant information for future astronomical molecular line surveys, as well as catalog the molecular complexity that is able to be produced from the processing of interstellar ices.

This work was supported by the W. M. Keck Foundation (M.J.A., B.M.J., R.I.K.). Partial support is also acknowledged from the National Aeronautics and Space Administration (NASA Astrobiology Institute under Cooperative Agreement No. NNA09DA77A issued through the Office of Space Science) (AB).

APPENDIX

First, the 10.49 eV photons were generated by exploiting the third harmonic (354.6 nm; 3.49 eV) of the 1064 nm (1.17 eV) fundamental of a Nd:YAG laser (Spectra Physics, PRO-250-30); the 354.6 nm (3.49 eV; 333 mJ per pulse) photon is then frequency tripled using pulsed jets of xenon (pulses of 80 μ s, 30 Hz) as a nonlinear medium to produce 118.2 nm (10.49 eV) light via non-resonant mixing (Maity et al. 2014b); this resulted in fluxes of typically 1.6×10^{14} photons per pulse (Figures 11–13). The operating pressure of the VUV generation chamber is typically 4×10^{-4} torr and the pulse valve is operated with a xenon backing pressure of 1900 torr. Second, the 9.60 eV photons were produced via four wave nonlinear difference mixing exploiting two photons of ω_1 and one photon of ω_2 (i.e., $2\omega_1 - \omega_2$) (Hilbig et al. 1986; Hepburn 1994). Here, UV (202.3 nm; 6.13 eV; ω_1) and visible (466.7 nm; 2.66 eV; ω_2) light was generated by separate Nd:YAG pumped dye lasers.

First, the 202.3 nm (6.13 eV; ω_1) light was generated utilizing a dye laser (Sirah, Cobra-Stretch) containing Rh 640 dye (Exciton), which was pumped by the second harmonic

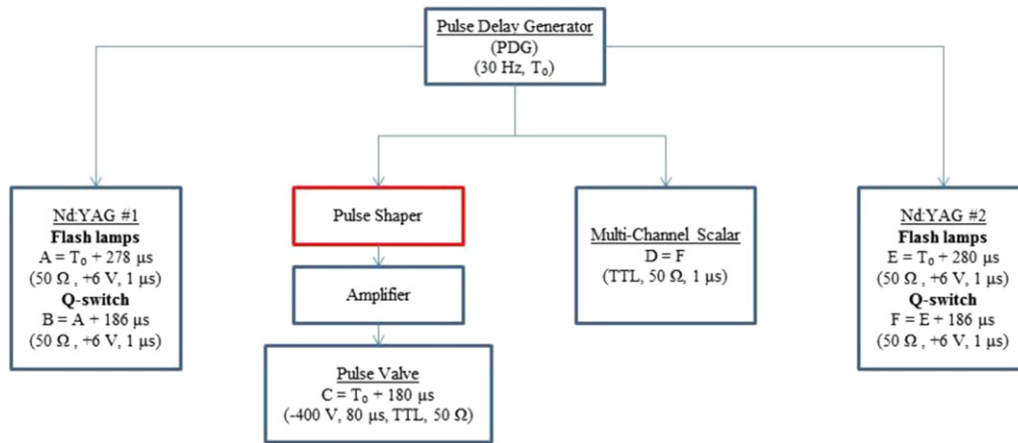


Figure 12. Schematic of the pulse sequence of the single photoionization reflectron time-of-flight mass spectrometer relative to the starting pulse operating at 30 Hz.

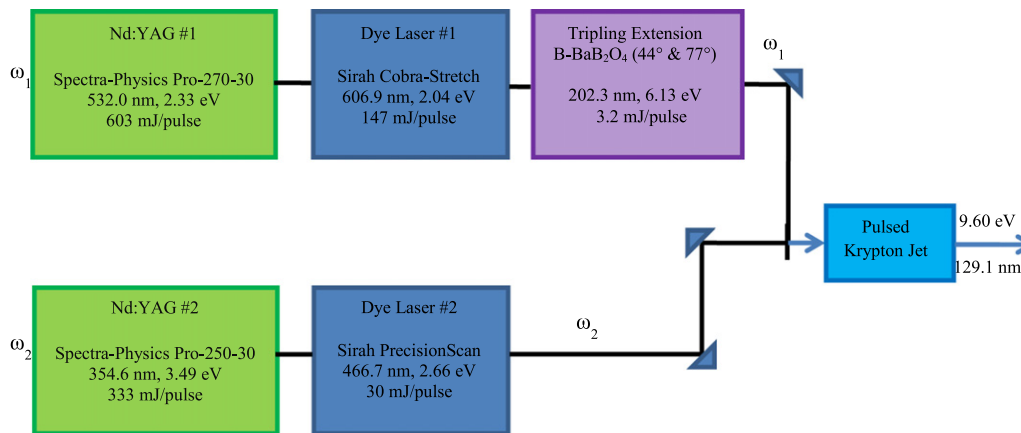


Figure 13. Top view schematic of the pulsed laser system used in the generation of coherent tunable vacuum ultraviolet light at 129.15 nm (9.60 eV) utilizing four wave nonlinear difference mixing ($2\omega_1 - \omega_2$; $\omega_1 = 202.3$ nm; $\omega_2 = 466.7$ nm). The different wavelengths are overlapped utilizing 90° prisms and a dichroic mirror that is reflective to 202.3 nm light and transparent to 466.7 nm light. The overlapping frequencies are then directed into the pulsed krypton gas jet and VUV light (9.60 eV) is produced.

(532 nm; 2.33 eV) of the fundamental of a Nd:YAG laser (1064 nm; 1.17 eV; Spectra Physics, PRO-270-30) and frequency tripling of the dye laser output (606.9 nm; 2.04 eV; 4.5×10^{17} photons per pulse) using β -BaB₂O₄ (BBO) crystals (44° and 77°). Overall fluxes of 3.3×10^{15} photons per pulse at 202.3 nm (6.13 eV) were achieved. Second, the 466.7 nm (2.66 eV; ω_2) light was produced by using the third harmonic (354.6 nm; 3.49 eV) of the 1064 nm (1.17 eV) fundamental of a Nd:YAG laser (Spectra Physics, PRO-250-30) at a power of 333 mJ per pulse to pump a dye laser (Sirah, Precision Scan) containing Coumarin 460 dye (Exciton) yielding 30 mJ per pulse (Figure 11).

Then, both ω_1 and ω_2 were focused by exploiting a fused silica bi-convex lens (Thorlabs LB4265; $f = 150$ mm), and were introduced through a MgF₂ window (Kurt J. Lesker Company; VPZL-275UM) into a differentially pumped vacuum chamber, which houses a pulsed piezoelectric valve. Operated at a backing pressure of 1520 torr, pulses of 80 μ s, and a repetition rate of 30 Hz, the pulsed valve introduces pulsed jets of krypton (99.999%; Specialty Gases), which serves as a nonlinear medium to generate the 9.60 eV VUV photons via difference four wave mixing from the photons of the spatially overlapping UV (202.3 nm; 6.13 eV; ω_1) and

visible (466.7 nm; 2.66 eV; ω_2) laser beams. Figure 12 compiles the pulse sequence used in the present experiments.

Briefly, the flash lamps for Nd:YAG #1 and Nd:YAG #2 are delayed with respect to time zero (T_0) utilizing channels A and E of the pulse delay generator (PDG) by 278 μ s and 280 μ s, respectively, for maximum overlap due to their difference in path length. The Q-switch of each Nd:YAG laser is synced to its respective flash lamp channel and delayed by 186 μ s. Note that the start trigger of the multi-channel scalar has the same delay as the Q-switch for Nd:YAG #2 as channel D is synced to channel F from the PDG. The output of pulse generator channel C (50 Ω , TTL, 80 μ s) is sent to a homemade pulse shaper which then leads to an amplifier that drove a piezoelectric valve at a rate of 30 Hz, -400 V amplitude, and 80 μ s duration. While Figure 13 portrays a schematic of the four wave nonlinear difference mixing experiments discussed above.

Note that this process generates UV light (202.3 nm, 6.13 eV, ω_1), visible light 466.7 nm, 2.66 eV, ω_2), and VUV light (83.1 nm, 14.92 eV, $2\omega_1 + \omega_2$; 129.15 nm, 9.60 eV, $2\omega_1 - \omega_2$; 67.4 nm, 18.39 eV, $3\omega_1$; 155.6 nm, 7.98 eV, $3\omega_2$), which in principle can all photoionize subliming molecules. The desired 9.60 eV photons are separated from the

“unwanted” light by using an off axis lithium fluoride (LiF) planoconvex lens (ISP Optics, LF-PX-38-150; $f=150$ mm) (VonDraese et al. 1988). Lithium fluoride does not transmit light above 105 nm (11.80 eV) thus absorbing the 14.92 eV and 18.39 eV light. Further, since the lithium fluoride lens has distinct refractive indices for different wavelengths, the off-axis location of the lens with respect to the incident photon beams results into a spatial separation of the 155.6 nm (7.98 eV, $3\omega_2$), 202.3 nm (6.13 eV, ω_1), and 466.7 nm (2.66 eV, ω_2) light, i.e., by 3.3, 5.3, and 7.1 mm from the focused 129.15 nm (9.60 eV, $2\omega_1 - \omega_2$) at a distance of 525 mm from the pulsed valve. The 129.15 nm (9.60 eV, $2\omega_1 - \omega_2$) light then passes through the 1 mm aperture of the copper plate and photoionizes the subliming molecules about 1 mm above the silver substrate. Two detectors were used to monitor and to optimize the generated VUV light and to ensure proper alignment of the VUV light through the main chamber. These detectors operate on the photoelectric principle and were constructed of high purity OFHC consisting of one solid disk with a diameter of 1.25 cm and thickness of 0.38 cm coupled to a ring with an inner diameter of 0.5 cm and separated using ceramic insulators (Maity et al. 2014b); with a total collection efficiency of this detector, the VUV is determined to be about 1.7×10^{14} photons per pulse for 129.15 nm (9.60 eV).

REFERENCES

- Adam, T., & Zimmermann, R. 2007, *Anal Bioanal Chem*, 389, 1941
- Bennett, C. J., Chen, S.-H., Sun, B.-J., Chang, A. H. H., & Kaiser, R. I. 2007, *ApJ*, 660, 1588
- Bennett, C. J., Jamieson, C., Mebel, A. M., & Kaiser, R. I. 2004, *PCCP*, 6, 735
- Bennett, C. J., Jamieson, C. S., & Kaiser, R. I. 2009, *PCCP*, 11, 4210
- Bennett, C. J., Jamieson, C. S., Osamura, Y., & Kaiser, R. I. 2005a, *ApJ*, 624, 1097
- Bennett, C. J., Jamieson, C. S., Osamura, Y., & Kaiser, R. I. 2006, *ApJ*, 653, 20
- Bennett, C. J., & Kaiser, R. I. 2007a, *ApJ*, 660, 1289
- Bennett, C. J., & Kaiser, R. I. 2007b, *ApJ*, 661, 899
- Bennett, C. J., Osamura, Y., Lebar, M. D., & Kaiser, R. I. 2005b, *ApJ*, 634, 698
- Bisschop, S. E., Fuchs, G. W., van Dishoeck, E. F., & Linnartz, H. 2007, *A&A*, 474, 1061
- Bohn, R. B., Sandford, S. A., Allamandola, L. J., & Cruikshank, D. P. 1994, *Icar*, 111, 151
- Breda, S., Reva, I., & Fausto, R. 2012, *JPCA*, 116, 2131
- Brock, A., Minacamilde, N., & Manzanares, C. 1994, *JPhCh*, 98, 4800
- Brown, R., Crofts, J., Godfrey, P., et al. 1975, *ApJL*, 197, L29
- Caldwell, R. A., & Cao, C. V. 1982, *JChS*, 104, 6174
- Caro, G. M. M., & Schutte, W. A. 2003, *A&A*, 412, 121
- Comeford, J., & Gould, J. H. 1961, *JMoSp*, 5, 474
- Cooper, D. M., & Langhoff, S. R. 1981, *JChPh*, 74, 1200
- Corkran, G., & Ball, D. W. 2004, *JMoSt*, 668, 171
- Coustenis, A., Schmitt, B., Khanna, R. K., & Trotta, F. 1999, *P&SS*, 47, 1305
- Cowieson, D. R., Barnes, A. J., & Orvillethomas, W. J. 1981, *JRSp*, 10, 224
- Cox, J. D., Wagman, D. D., & Medvedev, V. A. 1989, CODATA Key Values for Thermodynamics (New York: Hemisphere)
- de Marcellus, P., Meinert, C., Myrgorodska, I., et al. 2015, *PNAS*, 112, 965
- Dickens, J., Irvine, W. M., Nummelin, A., et al. 2001, *AcSpA*, 57, 643
- Dickens, J., Irvine, W. M., Ohishi, M., et al. 1997, *ApJ*, 489, 753
- Dows, D. A. 1962, *JChPh*, 36, 2833
- Drouin, D., Couture, A. R., Joly, D., et al. 2007, *Scanning*, 29, 92
- Ennis, C., Yuan, H. Q., Sibener, S. J., & Kaiser, R. I. 2011, *PCCP*, 13, 17870
- Frenkel, M. 1994, Thermodynamics of Organic Compounds in the Gas State, Vol. 1 (Boca Raton, FL: CRC Press)
- Fujii, S., Osaka, N., Akita, M., & Itoh, K. 1995, *JPhCh*, 99, 6994
- Gallaway, W., & Barker, E. 1942, *JChPh*, 10, 88
- Garozzo, M., Fulvio, D., Kanuchova, Z., Palumbo, M. E., & Strazzulla, G. 2010, *A&A*, 509, A67
- Geppert, W. D., Hamberg, M., Thomas, R. D., et al. 2006, *FaDi*, 133, 177
- Gibb, E. L., Whittet, D. C. B., Boogert, A. C. A., & Tielens, A. G. G. M. 2004, *ApJS*, 151, 35
- Gilmore, W., Morris, M., Palmer, P., et al. 1976, *ApJ*, 204, 43
- Goodman, A. M. 1978, *ApOpt*, 17, 2779
- Goulay, F., Trevitt, A. J., Savee, J. D., et al. 2012, *JPCA*, 116, 6091
- Groner, P., Stolkin, I., & Gunthard, H. H. 1973, *JPhE*, 6, 122
- Gurvich, L. V. 1989, *Pure Appl Chem*, 61, 1027
- Heavens, O. S. 1965, Optical Properties of Thin Solid Films (London: Scientific Publications Butterworths)
- Hepburn, J. W. 1994, Laser Techniques in Chemistry (New York: Wiley)
- Herbst, E. 2014, *PCCP*, 16, 3344
- Hilbig, R., Hilber, G., Lago, A., Wolff, B., & Wallenstein, R. 1986, *Proc. SPIE*, 613, 48
- Hollis, J. M., Jewell, P., Lovas, F., Remijan, A., & Møllendal, H. 2004, *ApJL*, 610, L21
- Hollis, J. M., Lovas, F. J., & Jewell, P. R. 2000, *ApJL*, 540, L107
- Hollis, J. M., Remijan, A. J., Jewell, P. R., & Lovas, F. J. 2006, *ApJ*, 642, 933
- Hudson, R., Gerakines, P., & Moore, M. 2014, *Icar*, 243, 148
- Hudson, R. L., & Moore, M. H. 1999, *Icar*, 140, 451
- Irvine, W. M., Brown, R. D., Cragg, D. M., et al. 1988, *ApJL*, 335, L89
- Jaber, A. A., Ceccarelli, C., Kahane, C., & Caux, E. 2014, *ApJ*, 791, 29
- Jamieson, C. S., Mebel, A. M., & Kaiser, R. I. 2006, *ApJS*, 163, 184
- Jiang, G. J., Person, W. B., & Brown, K. G. 1975, *JChPh*, 62, 1201
- Jones, B. M., & Kaiser, R. I. 2013, *JPhChL*, 4, 1965
- Jongma, R. T., Berden, G., & Meijer, G. 1997, *JChPh*, 107, 7034
- Kaiser, R. I. 2002, *ChRv*, 102, 1309
- Kaiser, R. I., Eich, G., Gabrys, A., & Roessler, K. 1997, *ApJ*, 484, 487
- Kaiser, R. I., Maity, S., & Jones, B. M. 2014, *PCCP*, 16, 3399
- Kaiser, R. I., Maity, S., & Jones, B. M. 2015, *Angew Chem Int Edit*, 54, 195
- Kaiser, R. I., & Roessler, K. 1997, *ApJ*, 475, 144
- Kaiser, R. I., & Roessler, K. 1998, *ApJ*, 503, 959
- Khare, B., Thompson, W., Murray, B., et al. 1989, *Icar*, 79, 350
- Kim, Y. S., Bennett, C. J., Li-Hsieh, C., Brien, K. O., & Kaiser, R. I. 2010, *ApJ*, 711, 744
- Kim, Y. S., & Kaiser, R. I. 2010, *ApJ*, 725, 1002
- Levin, I. W., Pearce, R. A., & Harris, W. 1973, *JChPh*, 59, 3048
- Maity, S., Kaiser, R. I., & Jones, B. M. 2014a, *ApJ*, 789, 36
- Maity, S., Kaiser, R. I., & Jones, B. M. 2014b, *FaDi*, 168, 485
- Maity, S., Kaiser, R. I., & Jones, B. M. 2015, *PCCP*, 17, 3081
- Mason, N. J., Dawes, A., Holtom, P. D., et al. 2006, *FaDi*, 133, 311
- Mehring, D. M., Snyder, L. E., & Miao, Y. T. 1997, *ApJL*, 480, L71
- Minh, Y. C., & van Dishoeck, E. F. 2000, in Astrochemistry: From Molecular Clouds to Planetary Systems, ed. Y. C. Minh (San Francisco, CA: ASP), 286
- Moore, M. H., Ferrante, R. F., & Nuth Iii, J. A. 1996, *P&SS*, 44, 927
- Moore, M. H., & Hudson, R. L. 1998, *Icar*, 135, 518
- Moore, M. H., & Hudson, R. L. 2005, in Proc. IAU Symp. 231, Astrochemistry: Recent Successes and Current Challenges, ed. D. C. Lis, G. A. Blake & E. Herbst (Cambridge: Cambridge Univ. Press), 247
- Moore, M. H., Hudson, R. L., & Gerakines, P. A. 2001, *AcSpe*, 57, 843
- Morton, R. J., & Kaiser, R. I. 2003, *P&SS*, 51, 365
- Nguyen, M. T., Matus, M. H., Lester, W. A., & Dixon, D. A. 2008, *JPCA*, 112, 2082
- Pochan, J., Baldwin, J., & Flygare, W. 1968, *JChS*, 90, 1072
- Puzzarini, C., Penocchio, E., Biczysko, M., & Barone, V. 2014, *JPCA*, 118, 6648
- Rawlings, J. M. C., Williams, D. A., Viti, S., & Cecchi-Pestellini, C. 2013, *MNRAS*, 436, L59
- Requena-Torres, M. A., Martín-Pintado, J., Martín, S., & Morris, M. R. 2008, *ApJ*, 672, 352
- Rodriguez, H. J., Chang, J.-C., & Thomas, T. F. 1976, *JChS*, 98, 2027
- Rothger, E., Holt, R., & McGee, H., Jr 1975, *JChS*, 97, 4971
- Rytter, E., & Gruen, D. M. 1979, *AcSpA*, 35, 199
- Shimanouchi, T. 1972, Tables of Molecular Vibrational Frequencies Consolidated, Vol. 1 (Gaithersburg, MD: National Bureau of Standards)
- Sigurbjornsson, O. F., & Signorell, R. 2008, *PCCP*, 10, 6211
- Simoes, J. M., Greenberg, A., & Liebman, J. F. 1996, Energetics of Organic Free Radicals, Vol. 4 (Dordrecht: Springer Science & Business Media)
- Socrates, G. 2004, Infrared and Raman Characteristic Group Frequencies: Tables and Charts (New York: John Wiley & Sons)
- Stein, S. E. 2010, Mass Spectra, ed. P. J. Linstrom & W. G. Mallard (Gaithersburg, MD: National Institute of Standards and Technology)
- Strazzulla, G., & Johnson, R. E. 1991, in Comets in the Post-Halley Era, ed. R. L. Newburn, Jr., M. Neugebauer & J. Rahe (Dordrecht: Springer Netherlands), 243
- Tejada, S. B., & Eggers, D. F. 1976, *AcSpA*, 32, 1557

- Turner, B. E., & Apponi, A. J. 2001, [ApJL](#), **561**, L207
- Ureña, F. P., Gómez, M. F., González, J. J. L., & Torres, E. M. N. 2003, [AcSpA](#), **59**, 2815
- van Nes, G. J. H. 1978, PhD thesis, Univ. Groningen
- VonDrasek, W. A., Okajima, S., & Hessler, J. P. 1988, [ApOpt](#), **27**, 4057
- Wada, A., Mochizuki, N., & Hiraoka, K. 2006, [ApJ](#), **644**, 300
- Wang, C. C., Lang, E. K., & Signorell, R. 2010, [ApJL](#), **712**, L40
- Wang, H. Y., Eyre, J. A., & Dorfman, L. M. 1973, [JChPh](#), **59**, 5199
- Watanabe, K. 1957, [JChPh](#), **26**, 542
- Werner, H.-J., Bauer, C., Rosmus, P., et al. 1995, [JChPh](#), **102**, 3593
- Xu, L. H., Jiang, X. J., Shi, H. Y., et al. 2011, [JMoSp](#), **268**, 136
- Zhou, L., Kaiser, R. I., Gao, L. G., et al. 2008, [ApJ](#), **686**, 1493
- Zhou, L., Maity, S., Abplanalp, M., Turner, A., & Kaiser, R. I. 2014, [ApJ](#), **790**, 38